A CLIMATOLOGY OF TROPICAL ANVIL AND ITS RELATIONSHIP TO THE LARGE-SCALE CIRCULATION

A Dissertation

by

WEI LI

Submitted to the Office of Graduate Studies of
Texas A&M University
in partial fulfillment of the requirements for the degree of

DOCTOR OF PHILOSOPHY

December 2009

Major Subject: Atmospheric Sciences

A CLIMATOLOGY OF TROPICAL ANVIL AND ITS RELATIONSHIP TO THE LARGE-SCALE CIRCULATION

A Dissertation

by

WEI LI

Submitted to the Office of Graduate Studies of
Texas A&M University
in partial fulfillment of the requirements for the degree of

DOCTOR OF PHILOSOPHY

Approved by:

Chair of Committee,	Courtney Schumacher
Committee Members,	R. Saravanan
	Shaima L. Nasiri
	Debbie Thomas
	Ian Kraucunas
Head of Department,	Kenneth Bowman

December 2009

Major Subject: Atmospheric Sciences

ABSTRACT

A Climatology of Tropical Anvil and Its Relationship to the Large-Scale Circulation.

(December 2009)

Wei Li, B.S., Nanjing Institute of Meteorology;

M.S., Chinese Academy of Meteorological Sciences

Chair of Advisory Committee: Dr. Courtney Schumacher

This dissertation uses multiple tools to investigate tropical anvil, i.e., thick, non-precipitating cloud associated with deep convection with the main objectives to provide a climatology of tropics-wide anvil properties and a better understanding of anvil formation, and to provide a more realistic assessment of the radiative impact of tropical anvil on the large-scale circulation. Based on 10 years (1998-2007) of observations, anvil observed by the Tropical Rainfall Measuring Mission (TRMM) Precipitation (PR) shows significant geographical variations, which can be linked to variations in the parent convection. Strong upper level wind shear appears to assist the generation of anvil and may further explain the different anvil statistics over land and ocean. Variations in the large-scale environment appear to play a more important role in anvil production in regions where convection regularly attains heights greater than 7 km. For regions where convection is less deep, variations in the depth of the convection and the large-scale environment likely contribute more equally to anvil generation.

Anvil radiative heating profiles are estimated by extrapolating millimeter cloud radar (MMCR) radiative properties from Manus to the 10-year TRMM PR record. When

the unconditional anvil areal coverage is taken into account, the anvil radiative heating becomes quite weak, increasing the PR latent heating profile by less than 1% at mid and upper levels. Stratiform rain and cirrus radiative heating contributions increase the upper level latent heating by 12%. This tropical radiative heating only slightly enhances the latent heating driven model response throughout the tropics, but more significantly over the East Pacific. These modest circulation changes suggest that previous studies may have overemphasized the importance of radiative heating in terms of Walker and Hadley circulation variations. Further, the relationship of cloud radiative heating to latent heating needs to be taken into account for more realistic studies of cloud radiative forcing on the large-scale circulation.

DEDICATION

To my father

To my husband Yonghui and our son Chutian

ACKNOWLEDGMENTS

I would like to first thank my advisor, Dr. Courtney Schumacher, for her always-enthusiastic, heuristic instruction and encouragement, which made my dissertation go smoothly and helped me build confidence, which is an invaluable treasure in my life. Other committee members, Dr. R. Saravanan, Dr. Shaima Nasiri, Dr. Ian Kraucunas, and Dr. Debbie Thomas, have offered many valuable comments on my research and encouragement during my study. Dr. Sally McFarlane provided millimeter cloud radar (MMCR) data, which significantly helped my radiative heating analysis. Dr. Qiang Fu offered valuable suggestions on my modeling results and Dr. Lee Panetta offered helpful suggestions on computational techniques to make my dissertation go more efficiently.

I have many thanks to Dr. Fuqing Zhang for his recommendation and longtime support for me to pursue my advanced graduate studies. My A-team peers always offered enthusiastic help and support whenever I needed it. I also benefited from the support of the staff of the Department of Atmospheric Science, who are patient, professional and responsible. Many colleagues, Shuguang Wang, Xiaojie Zhu, Guanglin Tang, contributed to the scientific discussion of my research. I especially thank Zhiyong (Ellie) Meng for her help and encouragement during hard times, and for her longtime sibling-like friendship. I would like to also especially thank Gang Hong for the many inspiring discussions. Interaction with my classmates and other friends in College Station also make my life at Texas A&M university memorable and enjoyable.

My family offered tremendous support during my study and my gratitude for them can hardly be expressed by words.

This research was sponsored by the ARM-DOE Grant DE-FG02-06ER64174.

TABLE OF CONTENTS

Page

CHAPTER Page

LIST OF TABLES

LIST OF FIGURES

FIGURE Page

FIGURE Page

FIGURE Page

CHAPTER I

INTRODUCTION

Tropical deep convection plays an important role in regulating the tropical circulation and energy and water budgets. The mature stage of a tropical convective cloud cluster consists of four parts: a) deep precipitating convective towers characterized by vigorous updrafts and downdrafts; b) stratiform precipitating cloud connected to the deep convection exhibiting weaker, mesoscale vertical motions, c) non-precipitating thick anvil attached to either the stratiform or convective precipitating areas, and d) cirrus – optically thin cloud detrained from any of the three previous cloud types. This dissertation focuses on the third category - non-precipitating thick anvil associated with deep convection.

1.1 Anvil characteristics

Studies that have discussed tropical anvil properties (Webster and Stephens 1980, Machado and Rossow 1993, Schumacher and Houze 2006, Frederick and Schumacher 2008, Cetrone and Houze 2009) suggest that anvil can play an important role in the water budget of a tropical convective system. Webster and Stephens (1980) first highlighted the large areal coverage of anvil during the Winter Monsoon Experiment (WMONEX) in Indonesia and the South China Sea. Machado and Rossow (1993) used International Satellite Cloud Climatology Project (ISCCP) data to look at the tropics-wide distribution of convective systems and the associated mesoscale anvil cloud area. However, these

---

This dissertation follows the style of *Journal of the Atmospheric Sciences.*

studies were limited in their ability to measure anvil vertical structure and did not separate the raining (i.e., stratiform rain region) from the non-raining areas, leaving large gaps in our understanding of tropical anvil.

The Tropical Rainfall Measuring Mission (TRMM) satellite was launched in November 1997 and the Precipitation Radar (PR) aboard it has the capability to detect the vertical structure of rainfall and thick anvil. The TRMM PR data have been widely used to investigate the macro properties of tropical convective systems (e.g., Nesbitt et al. 2000, Petersen and Rutledge 2001, Schumacher and Houze 2003). Based on PR observations over the East Atlantic and West Africa, Schumacher and Houze (2006) argued that stratiform rain regions may grow at the expense of anvil in situations of low upper level wind shear and high low-level humidity. By combining TRMM PR and CloudSat Cloud Profiling Radar (CPR) observations, Cetrone and Houze (2009) investigated anvil over West Africa, the Maritime Continent, and the Bay of Bengal and suggested that differences in thick anvil echo structure occur because West African anvil is more closely linked to its (graupel producing) convective core, while oceanic anvils tend to extend out from large stratiform rain areas.

Frederick and Schumacher (2008) used C-band polarimetric/Doppler Radar (C-POL) measurements to investigate anvil characteristics observed during the Tropical Warm Pool International Cloud Experiment (TWP-ICE) in Darwin during the Australian monsoon. They showed that the ratio of anvil area to rain area was 0.5 averaged throughout the field campaign and that anvil often lasted several hours after the parent convection had expired. In addition, they separated anvil into ice (i.e., echo base > 6 km) and mixed (i.e., echo base between 3 and 6 km) regions since the radiative properties of

both anvil types can be quite different. The average thickness of ice and mixed anvil was 2.8 and 6.7 km, respectively and anvil top heights ranged from 10-17 km. Mixed anvil usually formed in association with stratiform rain and typically preceded the peak in ice anvil.

Despite these studies, the tropics-wide occurrence and vertical extent of anvil remain unknown and the relationship of anvil to its parent convection is far from understood. This dissertation aims to further investigate anvil properties and links between anvil and its parent convection across the whole tropics using long-term TRMM PR and CloudSat CPR measurements.

1.2 Anvil radiative heating

The areal coverage and longevity of anvil implies that it may have a significant impact on the tropical circulation through its radiative effect. Webster and Stephens (1980) calculated the radiative heating profiles of middle and upper tropospheric optically thick cloud during WMONEX using a radiative transfer model. Their resulting cloud radiative profiles showed net heating (~10-20 K d^{-1}) near cloud base and net cooling (-1–-5 K d^{-1}) near cloud top. Ackerman et al. (1988) used satellite observations and aircraft measurements from a case study over Panama to obtain tropical anvil and cirrus heating rates from radiative transfer calculations. Their results showed that a 2-km thick anvil had a net heating rate of about 20 to 30 K d^{-1} and, similar to Webster and Stephens (1980), a large difference in heating rate existed between cloud top and bottom. However, the magnitude of heating is greater than in Webster and Stephens (1980). Machado and Rossow (1993) performed radiative transfer calculations to obtain the radiative heating profile of tropical convective systems across the tropics based on the

ISCCP data. Their results indicated anvil heating between 700 and 300 hPa and anvil cooling near 250h Pa. The maximum heating was around 5 K d^{-1} and maximum cooling was around -5 K d^{-1}. Their work compared the anvil radiative heating with the latent heating in the precipitating portion of the system and stressed that the anvil radiative effect dominated the total radiative effect of the convective system, in agreement with Houze's (1982) idealized diabatic heating budget of a tropical convective system based on observations during GATE in the East Atlantic. These studies provide general radiative characteristics of tropical anvil, but the geographical distribution of anvil macro properties are necessary before a more complete anvil radiative heating climatology can be created.

The TRMM PR provides extensive 3D information on tropical precipitation and thick cloud. However, the low sensitivity of the PR limits its ability to see any portion of the anvil that does not contain precipitation-size hydrometeors. The Department of Energy (DOE) Atmospheric Radiation Measurement (ARM) cloud radars in the tropical West Pacific allow high vertical and temporal resolution calculations of cloud radiative properties (Comstock et al. 2002, Comstock and Jakob 2004, McFarlane and Evans 2004a, b, Mather et al. 2007, McFarlane et al. 2007). By matching TRMM PR observations with cloud radiative information from the DOE ARM sites, this study will build a time series of anvil radiative properties across the tropics. An idealized climate model will then be used to examine the sensitivity of the large-scale circulation to the three-dimensional variation of anvil radiative heating.

1.3 Large-scale circulation

One of the major uncertainties in simulations of climate change is cloud feedbacks (e.g., changes in cloud height, cloud cover, and cloud optical thickness in a warming atmosphere, Colman 2003, Stephens 2005, Clement and Soden 2005). Better understanding of the climatological variation of tropical anvil and its relationship to deep convection can potentially improve relevant general circulation model (GCM) parameterizations. For instance, Randall et al. (1989) investigated cloud radiative forcing (CRF) and its interaction with large-scale dynamics in a GCM and highlighted the importance of assessing the GCM's cloud generation processes with observations. Krueger et al. (1995) also stressed the importance of realistic simulation of tropical anvil properties (e.g., extent and other microphysical properties) because of the radiative significance of anvil. Zender and Kiehl (1997) tested the climate sensitivity of the anvil representation (diagnostically or prognostically) in the National Center for Atmospheric Research (NCAR) Community Climate Model (CCM) and found that the upper tropospheric temperature structure, Hadley circulation, tropical deep convection, and northern hemisphere wintertime flow field were all sensitive to the anvil and cirrus characteristics; therefore, they also stressed the importance of anvil representation in GCM cloud parameterizations. Yao and Del Genio (1999) compared the climate feedback obtained from doubled CO_2 experiments with different parameterizations of large-scale clouds and moist convection by using the Goddard Institute for Space Studies (GISS) GCM. They showed that the presence of optically thick anvil clouds reduces the climate sensitivity by about 0.6 ºC. However, it is very difficult to represent anvil formation processes in GCMs. Therefore, they suggested using a semi-empirical approach based on

statistical relationships derived from satellite data and cloud resolving models to reduce uncertainty.

Previous work concerning the impact of the CRF (i.e., the difference in radiation budget components between clear and cloudy skies) of mid- to upper tropospheric cloud suggests a possible effect of tropical thick anvil on the large-scale tropical circulation (Webster and Stephens 1980, Ackerman et al. 1988, Randall et al. 1989, Ramaswamy and Ramanathan 1989, Ramanathan et al. 1983, Slingo and Slingo 1991, Sherwood et al. 1994, Lohmann and Roeckner 1995, Bergman and Hendon 2000 , Schumacher et al. 2004). For example, Sherwood et al. (1994) using a GCM showed that the Hadley and Walker circulations weaken when the radiative heating associated with tropical upper tropospheric cloud is excluded. Bergman and Hendon (2000) performed a more realistic set of GCM simulations based on ISCCP radiative heating profiles (that still lack much vertical cloud information) and indicated that tropical CRF strengthens the latent heating driven large-scale circulation. However, a more realistic study has not been done due to a lack of observationally based cloud radiative heating profiles with high vertical resolution.

Although these works discuss the sensitivity of the large-scale circulation to horizontal variations in tropical cloud (including thick anvil), the large-scale dynamical response to the anvil cloud in isolation and to the variation of vertical structure in radiative heating of tropical anvil has not been studied. Houze (1982) argued that the diabatic heating associated with tropical cloud clusters has an elevated maximum compared to a purely convective heating profile. Houze pointed out that latent heating from stratiform precipitation and radiative heating from anvil and cirrus cloud both

contribute significantly to the elevated heating maximum. Hartmann et al. (1984) input an idealized heating profile from a mature cloud cluster based on Houze (1982) into a linearized primitive equation model. The model produced a more realistic Walker circulation with a westward tilt of mass flux with height. However, this feature did not occur in the simulation using a convective-only profile. In addition, Hartmann et al. (1984) found that the elevated tropical heating could lead to a reinforcement of the mid-latitude response.

Schumacher et al. (2004) used three years of TRMM PR data to more realistically represent the geographical and temporal variations of latent heating associated with varying contributions from stratiform rain. They found that increasing the stratiform rain fraction from 0 to 70% raised the latent heating maximum from 4.5 to 7.8 km, equivalent to the height changes from 600 to 400 hPa in Hartmann et al.'s (1984) idealized heating profiles. However, the tropics-wide stratiform rain fraction is 40% (Schumacher and Houze 2003), which produces a latent heating maximum at 6.5 km. Thus, the radiative heating from anvil and cirrus must account for the further elevation of the tropical cloud cluster diabatic heating profile necessary for a realistic response. This study will use an idealized version of the NCAR Community Atmosphere Model (CAM3) and the TRMM PR-estimated anvil radiative heating profiles to test the sensitivity of the large-scale circulation to tropical anvil.

There are two main objectives of this doctoral research: 1) provide a climatology of tropics-wide anvil properties and a better understanding of anvil formation, and 2) provide a more realistic assessment of the radiative impact of tropical anvil on the large-scale circulation.

CHAPTER II

DATA AND METHODOLOGY

This chapter describes the TRMM PR observations used in this dissertation. Since 'anvil' is not an explicit classification in the TRMM product suite, this chapter describes the reprocessing of TRMM PR data to isolate anvil echo. The TRMM PR has a relatively low sensitivity, so the later part of this chapter discusses the uncertainty in detecting anvil with the TRMM PR, which is a necessary consideration for the radiative heating estimates described in Section 5.1.

2.1 TRMM precipitation radar

The TRMM PR is the first spaceborne precipitation radar and started collecting data December 1997 (Kummerow et al. 1998, Kozu et al. 2001). The TRMM satellite is still in orbit providing a ten-plus year dataset. The PR has a frequency of 13.8 GHz and operates at K_u band (2.17 cm wavelength) with a sensitivity ~17 dBZ (18 dBZ after the August 2001 orbit boost). The horizontal and vertical resolution of the PR is 4.3 km (5 km post-boost) and 250 m at nadir, which is sufficient to capture individual convective features and their vertical structure. This study uses TRMM product 2A25 (version 6) orbital data from 1 January 1998 to 31 December 2007, which includes the attenuation-corrected reflectivity and a copy of the rain type from TRMM product 2A23. The data covers the whole tropics and part of the subtropics (38°S – 38°N).

2.2 Anvil definition

TRMM product 2A23 takes into account both the vertical and horizontal

variability in the observed reflectivity field to classify radar echo as convective rain, stratiform rain, or other (Awaka et al, 1997). The 'other' category may include either noise or echo aloft not reaching the surface of the earth. Some of this echo aloft is attached to convective or stratiform rain echo (Schumacher and Houze 2006, Frederick and Schumacher 2008).

In this study, anvil is defined as echo with a 2A23 rain type equal to 160, 170, or 300, reflectivity > 17 dBZ, and an echo base higher than 3 km. The orbital data is grouped into 2.5°×2.5° daily grid boxes within a 35°S –35°N domain. At least 20 pixels in a grid box are required before statistics are calculated to guarantee that the selected anvil is not noise.

This dissertation subsets anvil into ice only and mixed ice/water categories because these anvil subtypes have significantly different radiative heating profiles and may represent different anvil evolution processes. The subtype definitions are based on Frederick and Schumacher (2008). Ice anvil has an echo base ≥ 6 km, while mixed anvil has an echo base between 3 and 6 km and an echo top ≥ 6 km to guarantee that part of the anvil is composed of ice (this threshold is based on the assumption that PR-observed echo bases are approximately the same as observed by C-POL since sedimentation leads to the largest particles at cloud base). It should be stressed that only anvil composed of large enough hydrometeors can be detected by the PR because of its low sensitivity (~17 dBZ). Therefore, anvil in this study refers to the thick anvil observable by the PR.

2.3 TRMM PR echo top and area correction

Due to the low sensitivity of the TRMM PR, PR-observed anvil may be underestimated in both the vertical and horizontal. The CPR aboard CloudSat is a 94-

GHz, nadir-viewing radar with a sensitivity ~-26 dBZ (Stephens et al. 2002). Its footprint is ~1.3 km (across track) x 1.7 km (along track) and it has a vertical resolution of 250 m, providing high-resolution observations of cloud structure.

This dissertation utilizes the 2D-CLOUDSAT-TRMM product (v1.0) during 1 August 2006-31 December 2008 to investigate the missing part of anvil viewed by the TRMM PR. During the available data period, there are about 6061 files with a TRMM/CloudSat intersection between 20°N and 20°S. The files include reflectivity from both radars as well as the rain type from TRMM product 2A23, making it possible to find the TRMM-derived anvil position in CPR observations. Out of 6061 intersect files, there are 332 (5.5%) cases that include PR-defined anvil. After marking the anvil on both radar tracks (an example overpass image is shown in Fig. 2.1), the difference of the echo top between the CloudSat CPR and TRMM PR is calculated. The PR echo top is the height of the 20-dBZ echo (or “storm height”) and the CPR echo top is the height of the -24-dBZ echo (or “cloud top”). Statistics show that the PR underestimates anvil top from 1 to 10 km with an average of ~5 km compared to the CPR (Fig. 2.2a). Casey et al. (2007) investigated the cloud-top difference between the TRMM PR and Geoscience Laser Altimeter System (GLAS) aboard the Ice, Cloud, and land Elevation Satellite (ICESat) and an analysis of the cloud-top difference in anvil based on his dataset also shows that the PR underestimates cloud top by ~5 km compared to the ICESat lidar.

In addition, the PR will miss anvil in the horizontal. This study collected 229 pair of coincident PR/CPR images with substantial anvil present and then subjectively compared the difference in anvil horizontal extent between CloudSat and the TRMM PR. Anvil observed by CloudSat is defined as echo with a base between 3 and 8 km and at

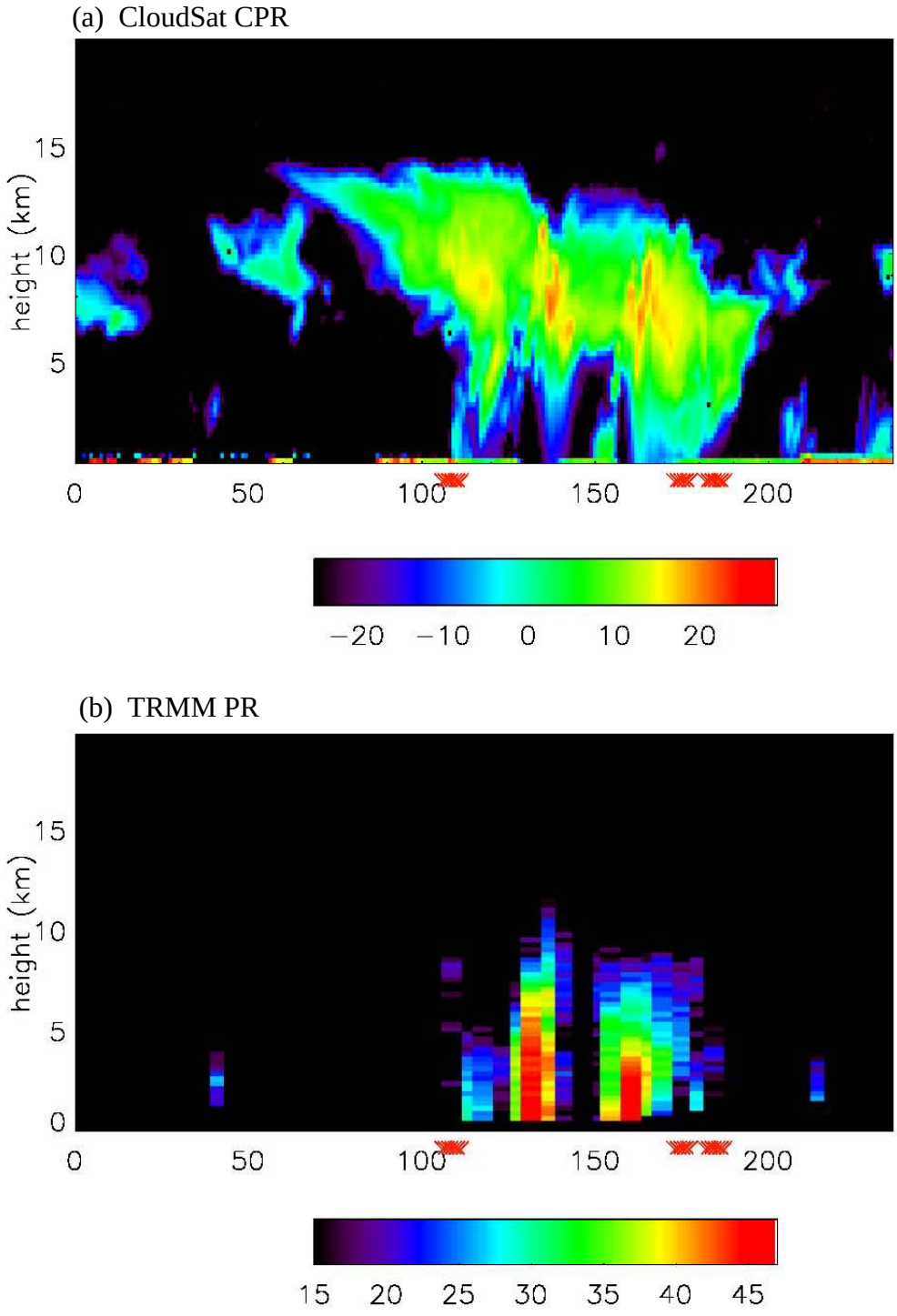

Figure 2. 1 Vertical cross sections of a coincident overpass for the (a) CloudSat CPR and (b) TRMM PR with PR-defined anvil marked as red 'x' in both images. The abscissa is the along track bins. The scan time of the images is around 19:23 local time on 10 August 2007. CloudSat is about 5 minutes in front of TRMM with the track centered at 19.85˚N, 87.93˚W. The color bars are reflectivity in dBZ.

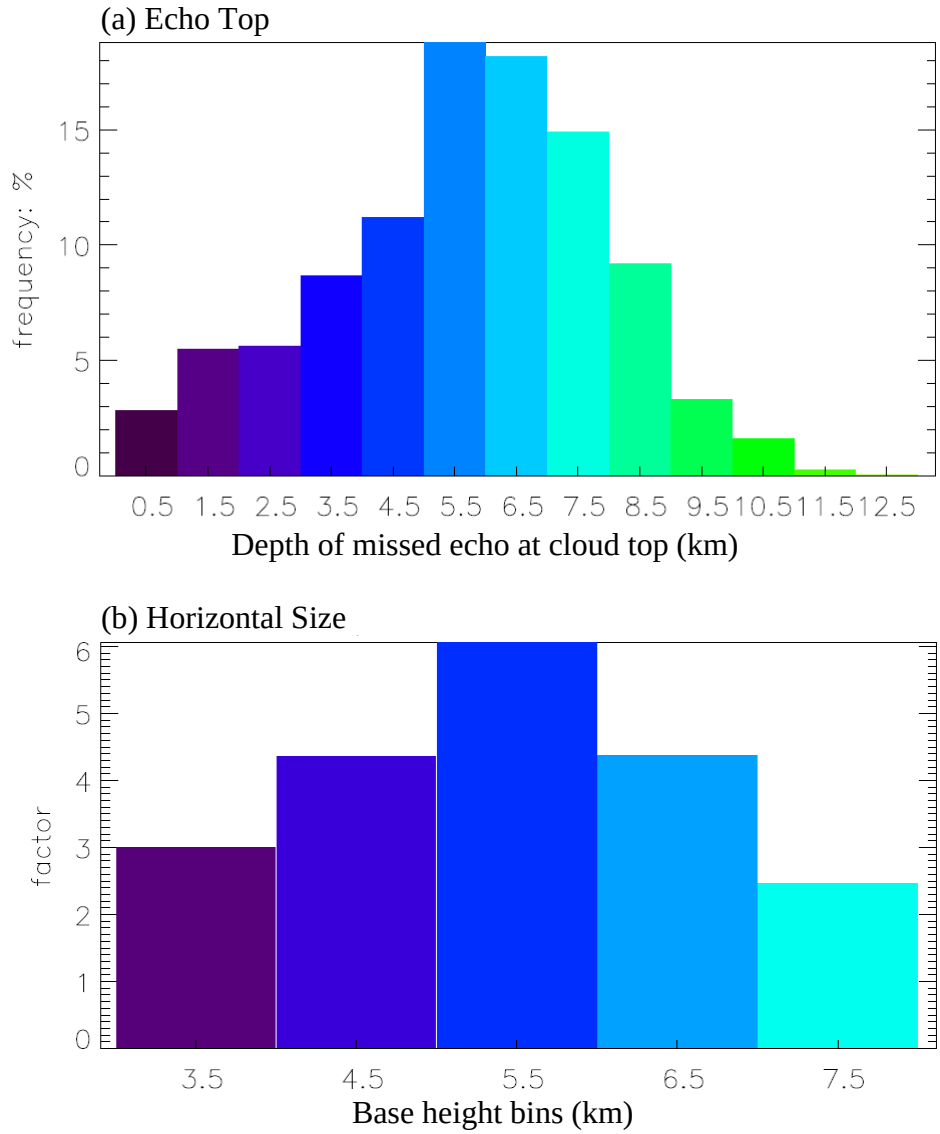

Figure 2. 2 (a) Frequency distribution of how much echo the PR is missing at cloud top and (b) the area factor the PR is missing in the horizontal compared to CloudSat. Echo top statistics are based on 3345 samples in along-track bins. Horizontal size statistics are based on 229 pairs of coincident PR/CPR images.

least 3 km thick primarily based on the CloudSat classifications in Riley and Mapes (2009). The horizontal area factor being missed by the TRMM PR is defined as: PR missing anvil/PR identified anvil. In the CPR dataset, cloud is sometimes defined as anvil but is not obviously associated with deep convection so is excluded from the PR comparison. Figure 2.2b shows that the PR underestimates anvil area by a factor of 3 to 8 with an average factor of ~4 compared to the CPR. The vertical and horizontal corrections are not added to the PR anvil climatology in the following two chapters, but will be explicitly taken into account in the anvil radiative heating calculations in chapters IV and V.

CHAPTER III

ANVIL CLIMATOLOGY

This chapter primarily discusses the 10-year spatial distribution of TRMM PR anvil macro properties (i.e., anvil occurrence, areal coverage, and vertical extent) and the associated temporal variability of these properties. The objective is to provide a comprehensive climatology of anvil observed by the TRMM PR.

3.1 Anvil occurrence

Anvil occurrence is defined as days with anvil within a 2.5˚×2.5˚ grid divided by the total number of days that the PR reported observations during 1998 to 2007. Anvil observable by the PR occurs around 5% of the time across the tropics with distinct geographical variability (Fig 3.1). In the tropics, anvil most commonly occurs over Africa, the Maritime Continent, and Panama (i.e., about 9% of the time). The frequent occurrence of anvil over these regions is consistent with Webster's (1983) definition of these regions as semipermanent equatorial convective zones that are not as affected by seasonal shifts in convection, unlike monsoon and intertropical convergence zone (ITCZ) regions that have lower anvil occurrence (i.e., about 3-4% of the time). Anvil also frequently occurs at higher latitudes in part because of the more frequent sampling of the TRMM satellite but also because anvil can be prevalent in midlatitude frontal systems.

3.2 Anvil areal coverage

Anvil areal coverage is defined as the number of anvil columns observed by the TRMM PR divided by the total number of PR columns (both with and without echo) in

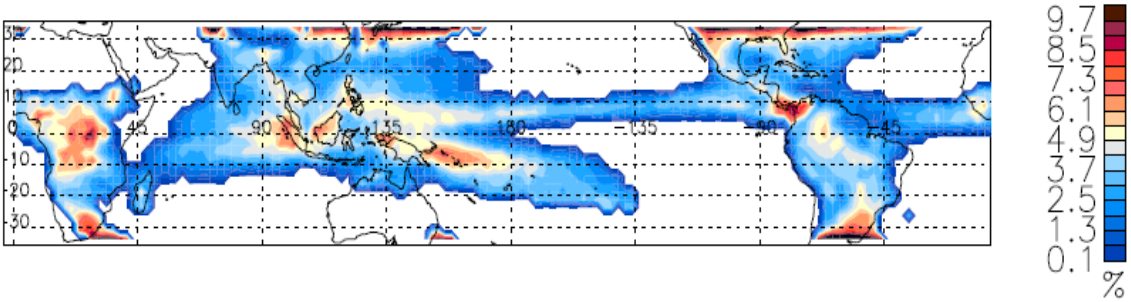

Figure 3. 1 TRMM PR anvil occurrence based on 2.5˚ grid averages for 1998-2007. Areas with deep convective rain (i.e., echo tops ≥ 9 km) occurrence less than 5% were not included. The same threshold is applied to most maps in chapters III and IV.

the grid box, times 100. Conditional values represent the average percent a grid box is covered by anvil when anvil is present, unconditional values represent the average percent a grid box is covered by anvil regardless of whether anvil is present. Figure 3.2a shows that the conditional anvil areal coverage is larger over land and smaller over ocean. For example, anvil areal coverage is 2-3% over Africa and South America, but only about 1% over the West Pacific warm pool. Recall from chapter II that these values need to be multiplied by five to account for the anvil area not sensed by the TRMM PR. The high areal coverage of anvil over Africa, northern Australia, and parts of Central and South America suggests that these regions are effective in producing large amounts of anvil per unit convection. The opposite is true over much of the tropical oceans. The efficiency of convection in producing anvil will be further explored in chapter IV.

Figures 3.2b and c show the geographical distribution of conditional anvil areal coverage separated into ice and mixed subtypes. Ice anvil accounts for about a third of the total anvil area and has higher areal coverage over land (0.5-1%) than ocean (0-0.5%). Similarly, mixed anvil has higher areal coverage over land (1-2%) than ocean (0.5-1%). In the tropical belt, ice and mixed anvil areal coverage is maximum over Africa where convection has been observed to be the deepest and most intense in the tropics (Petersen and Rutledge 2001, Alcala and Dessler 2002, Schumacher and Houze 2003, Zipser et al. 2006). The lower anvil amounts over the tropical oceans may also be due to the preference of stratiform rain to form at the expense of anvil since the ocean boundary layer is warm and humid with a weak diurnal cycle, which is favorable for the sustainability of convection and stratiform rain production (Schumacher and Houze 2003, Schumacher and Houze 2006).

(a) Anvil

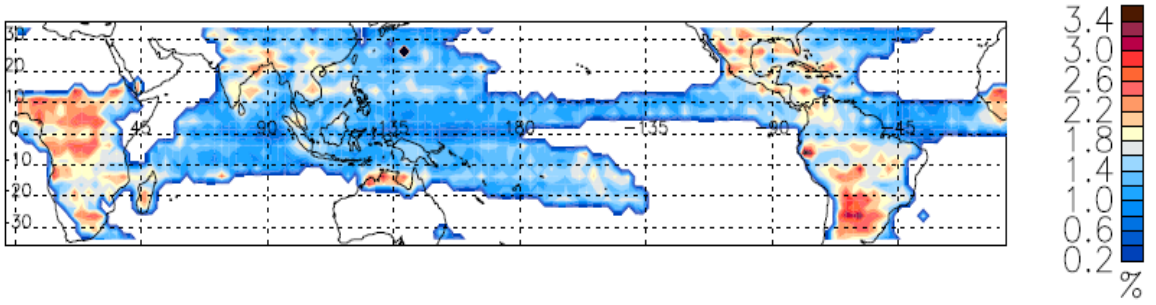

(b) Ice anvil

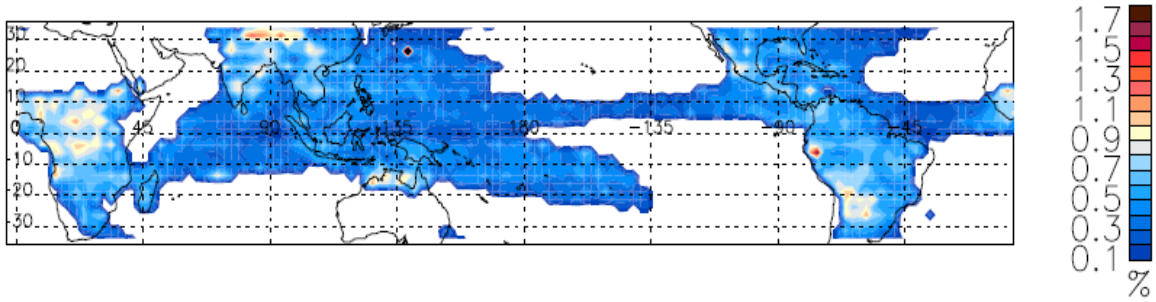

(c) Mixed anvil

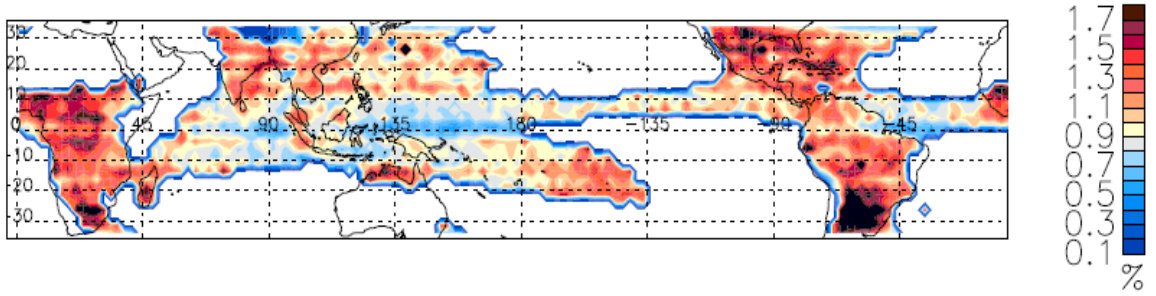

Figure 3. 2 Conditional TRMM PR areal coverage for (a) anvil, (b) ice anvil, and (c) mixed anvil based on 2.5˚ grid averages for 1998-2007.

The unconditional anvil areal coverage geographical distribution is shown in Fig. 3.3, since it is used to calculate the tropics-wide anvil radiative heating field. Maxima of more than 0.3% occur over central Africa and Panama. Again, recall that these values should be approximately multiplied by five for a more realistic estimate of how much area of the tropics is covered by anvil. Secondary maxima of about 0.2% occur over West Africa, the Maritime Continent, and the Amazon basin, while ocean values are closer to 0.1%.

3.3 Anvil vertical extent

Grid-averaged anvil echo tops range from 8 to 9.5 km (Fig. 3.4a) with a tropics-wide average of 8.5 km (Table 3.1). Frederick and Schumacher (2009) found that anvil echo tops ranged between 10 and 17 km during the Australian monsoon based on more sensitive C-POL observations, so after the echo top correction of 5 km these values appear reasonable. In addition, anvil is generally higher over land than ocean by 0.5 km. However, Cetrone and Houze (2009) found that anvil observed by CloudSat tended to be higher over ocean, so land convection appears to produce larger hydrometeors at higher heights but smaller particles are not lofted as high. When separated into subtypes, ice anvil echo tops range from 9 to 10 km (Fig. 3.4b) with a tropics-wide average of 9.3 km (Table 3.1), while mixed anvil echo tops are lower, ranging from 7.7 to 9 km (Fig. 3.4c) with a tropics-wide average of 8.3 km (Table 3.1). Land/ocean echo top differences within the ice and mixed subtypes are also ~0.5 km.

Grid-averaged anvil is 2.4-3.1 km thick (Fig. 3.5) with a tropics-wide average of 2.7 km (Table 3.1). Anvil is also thicker over land than ocean by 0.3 km. While ice anvil

(a) Anvil

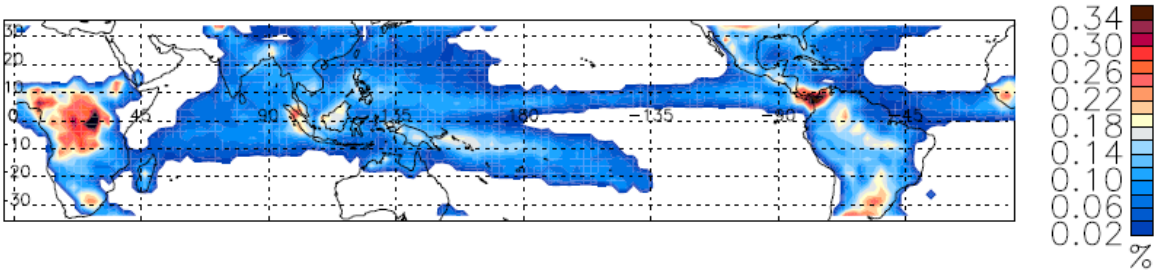

(b) Ice anvil

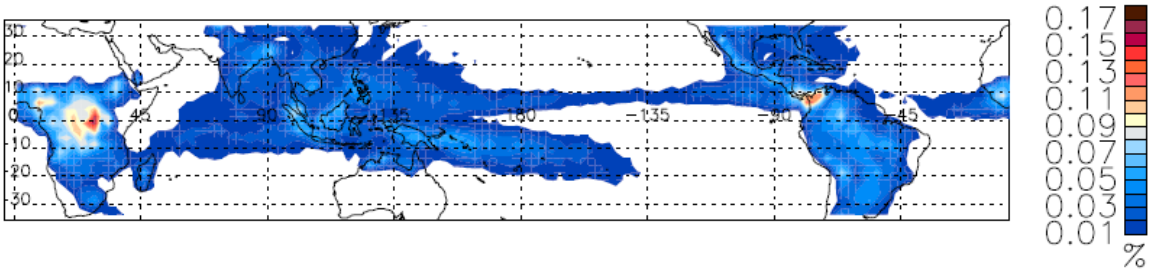

(c) Mixed anvil

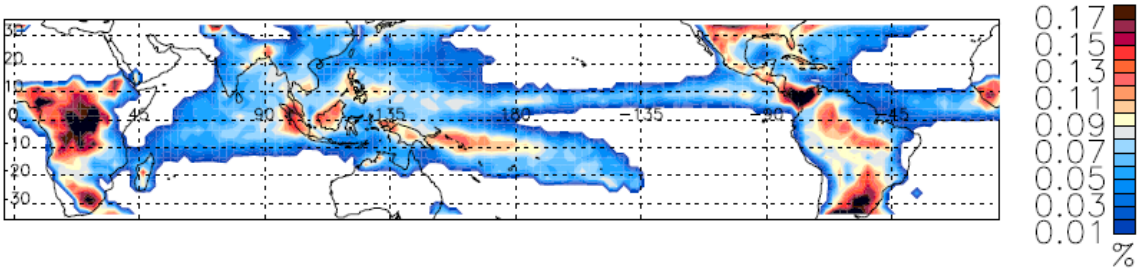

Figure 3. 3 Unconditional TRMM PR areal coverage for (a) anvil, (b) ice anvil, and (c) mixed anvil based on 2.5˚ grid averages for 1998-2007.

(a) Anvil

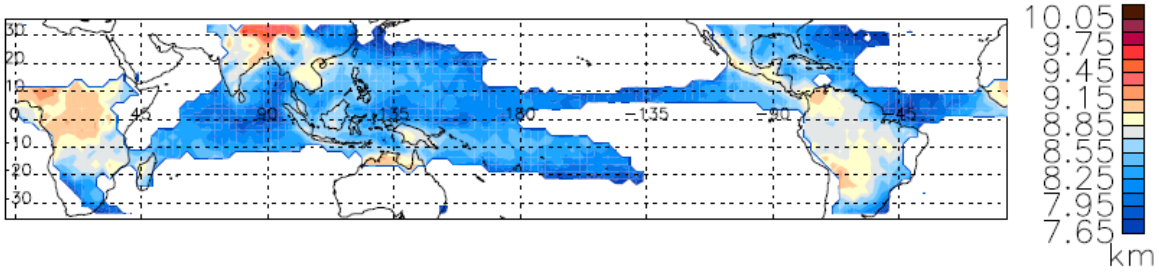

(b) Ice anvil

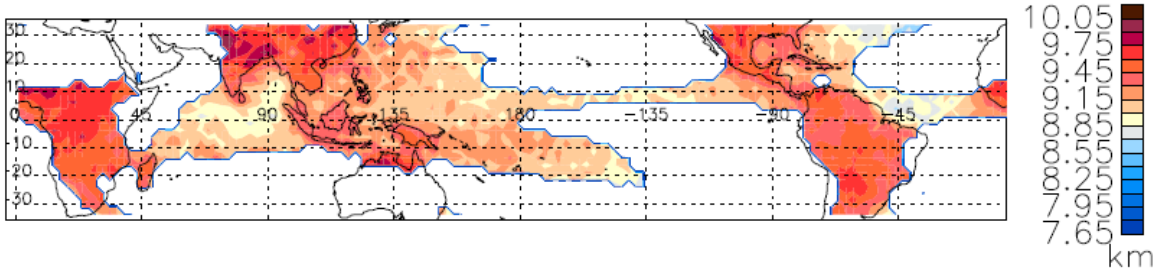

(c) Mixed anvil

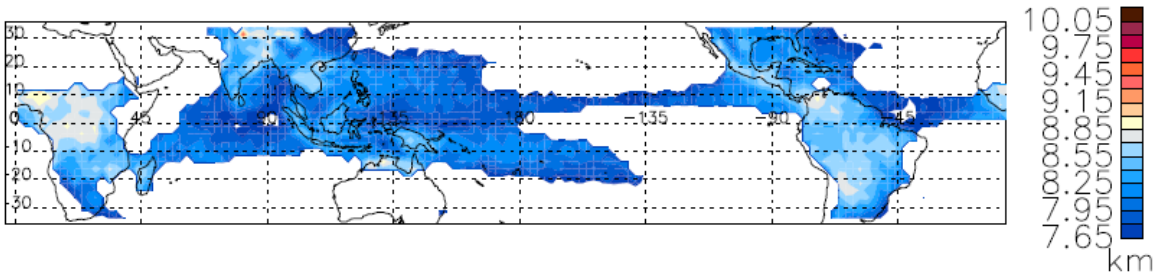

Figure 3. 4 TRMM PR mean echo tops for (a) anvil, (b) ice anvil, and (c) mixed anvil based on 2.5˚ grid averages for 1998-2007.

Table 3.1 Anvil vertical extent (in km) across the tropics (20°S-20°N).

	Anvil type	**Land**	**Ocean**	**Overall**
Top	Ice	9.5	9.2	9.3
	Mixed	8.5	8.1	8.3
	Overall	8.8	8.3	8.5
Base	Ice	7.9	7.9	7.9
	Mixed	5.0	4.9	5.0
	Overall	5. 9	5.7	5.7
Thickness	Ice	1.6	1.3	1.4
	Mixed	3.5	3.1	3.2
	Overall	2.9	2.7	2.7

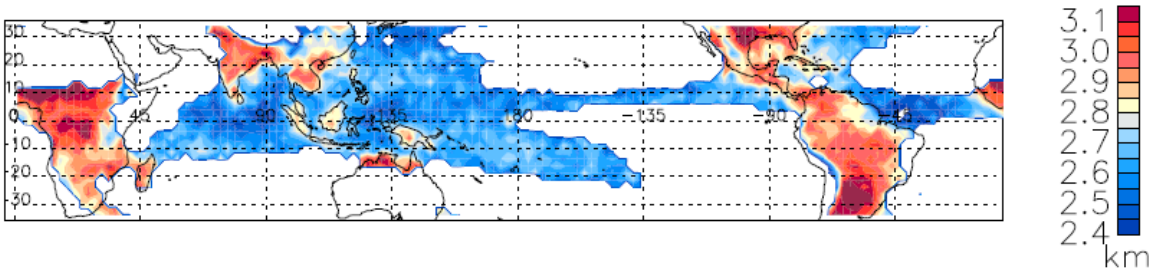

Figure 3. 5 TRMM PR mean anvil thickness based on 2.5˚ grid averages for 1998-2007.

is higher than mixed anvil, it is also thinner (Table 3.1). Climatologically, PR-observed ice anvil is 1.4 km thick, while PR-observed mixed anvil is 3.2 km thick. Again, land/ocean thickness differences within the ice and mixed subtypes are similar to the overall anvil thickness difference of 0.3 km. The vertical extent of anvil is likely determined by the vertical extent and intensity of the parent convection. In addition, large-scale upper level wind shear and mid-level moisture also may play an important role. These topics will be discussed in chapter IV.

3.4 Temporal variability in thick anvil

a. Seasonal variability

The ITCZ experiences a seasonal north-south migration and monsoon regions, by definition, experience significant seasonal variability. Since tropical anvil results from deep convection, it is necessary to investigate the significance of seasonal variability in anvil macro-properties.

As shown in Fig. 3.6 anvil conditional areal coverage, echo top, and thickness experience varying degrees of seasonal variability over the tropics. The most clear signal of seasonal variability occurs in echo top (Fig. 3.6b) with variations of more than 1 km over South Asia, northern Australia, and Mexico, all of which are affected by monsoon circulations. Anvil areal coverage (Fig 3.6a) shows a noisier pattern with heightened variability on the order of 1% over Africa in addition to parts of South Asia, northern Australia, and Central and South America. Anvil thickness (Fig. 3.6c) shows very little seasonal variability. It is interesting to note that while echo tops do not vary seasonally over Africa, areal coverage does, while the opposite is true over China. These differences

(a) Areal coverage

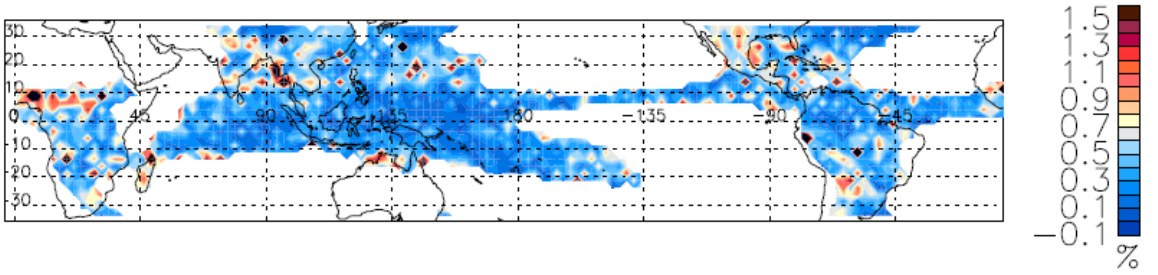

(b) Echo top

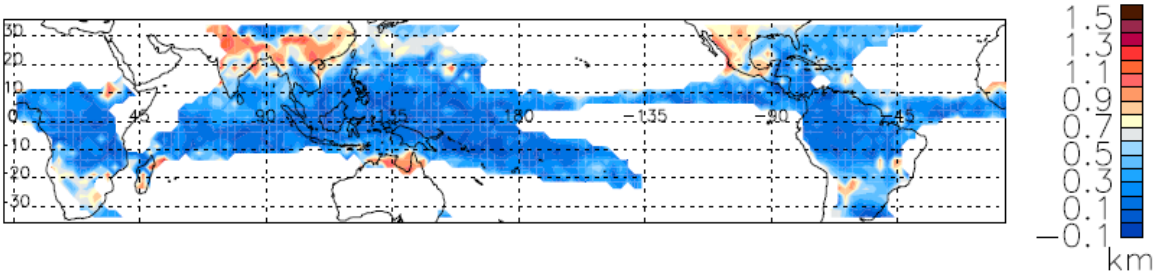

(c) Thickness

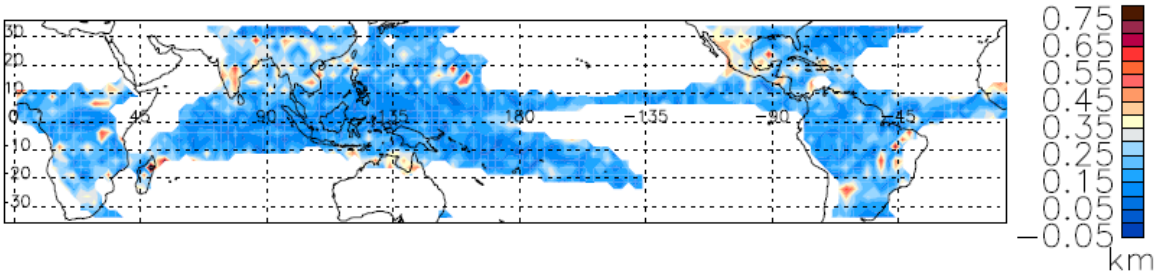

Figure 3. 6 Standard deviation of seasonal variability for TRMM PR anvil (a) conditional areal coverage, (b) echo top, and (c) thickness based on 2.5˚ grid averages for 1998-2007.

could be related to the seasonal variation of the parent deep convection or of the large-scale environment.

b. Inter-annual variability

The El Niño and Southern Oscillation (ENSO) is a coupled atmosphere-ocean phenomenon with a 3-6 year period (Trenberth 1997), which makes it the focus of climate change on inter-annual time scales. Several atmosphere-ocean components (sea surface temperature (SST), surface pressure, surface wind, precipitation, etc.) reflect the anomaly of this phenomenon. Being sensitive to SST, tropical convection also responds to ENSO (Rasmusson and Wallace 1983 among many other studies). Since thick anvil is closely associated with tropical convection, an ENSO signal in anvil occurrence would be expected.

Based on the NOAA multivariate ENSO index (MEI), four abnormally warm and four abnormally cold ENSO events were identified (Table 3.2). The average anvil occurrence map for the cold events was then subtracted from the average anvil occurrence map for the warm events (Fig. 3.7a). Anvil occurs 2-8% more often in the central and eastern Pacific and 5% less often in the far West Pacific during El Niño compared to La Niña. This pattern is consistent with the variability of deep convection (in this case convection with echo tops > 7 km) occurrence during ENSO (Fig. 3.7b). The conditional anvil area anomaly (not shown) did not indicate an ENSO signal; therefore, it is speculated that anvil occurrence (through increased or decreased occurrence of convection) is more sensitive to SST changes than anvil areal coverage (cf. Lindzen et al. 2001, which argues the opposite).

Table 3.2 Selected ENSO events during 1998-2007.

Warm events	**Cold events**
Jan – Apr 1998	Jan – Apr 1999
Nov 2002 – Apr 2003	Nov 1999 – Apr 2004
Nov 2004 – Mar 2005	Nov 2000 – Mar 2001
Nov 2006 – Mar 2007	Aug 2007 – Dec 2007

(a) Anvil

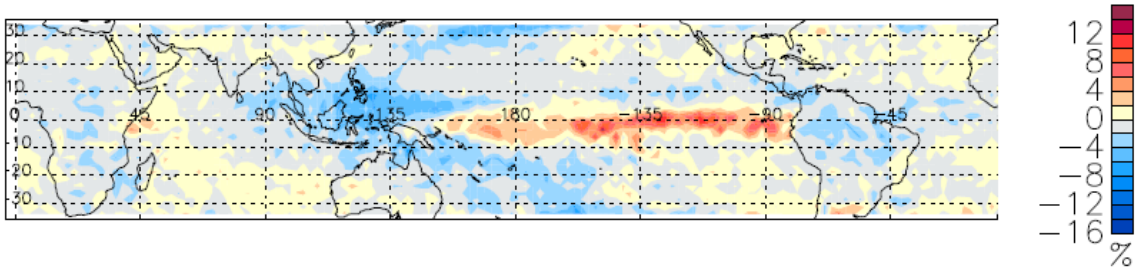

(b) Convective rain

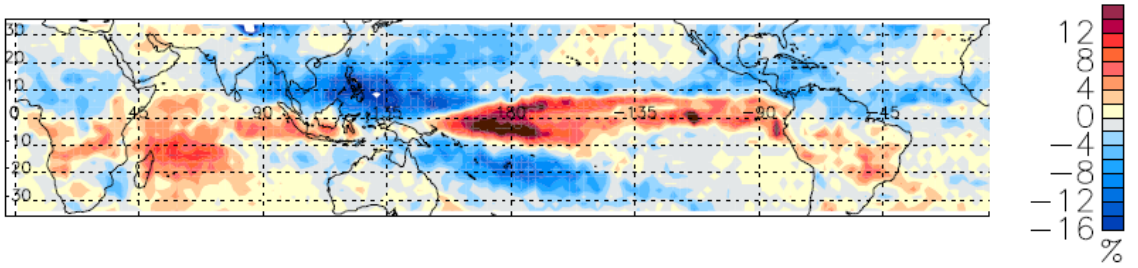

Figure 3. 7 TRMM PR (a) anvil and (b) deep convective rain (echo tops > 7 km) occurrence anomalies for El Nino-La Nina events during 1998-2007 (events are listed in Table 3.2) based on 2.5˚ grid averages.

CHAPTER IV

FACTORS AFFECTING ANVIL GENERATION AND EVOLUTION

Anvil, by definition, is associated with deep convection, but very little work has been done to quantify the relationship between anvil and its parent convection or how the large-scale environment affects anvil formation and evolution. Investigation of these issues will help to better understand the processes necessary for anvil production, which also provides useful information for model evaluation and parameterization improvement. Thus, this chapter discusses the quantitative relationship of anvil to deep convective and stratiform rain regions. This chapter also examines the difference in the large-scale relative humidity and zonal wind fields between days with and without anvil.

4.1 What kind of convection generates thick anvil?

Convective rain viewed by the TRMM PR occurs about 35% of the time in daily grids of 2.5º resolution (not shown). Some of these convective cells may generate thick anvil, while some will not due to factors such as the height of the convection, the convective intensity, or the size of the precipitating portion of the convective system.

To investigate the relationship between convective height and anvil generation, the average echo top of deep convective rain in the presence of anvil (Fig. 4.1a) and in the absence of anvil (Fig. 4.1b) was calculated. Convection that generates thick anvil is usually, on average, at least 7 km high, which is logical since anvil requires sufficient ice from the convective region to form and grow. Anvil-producing convection is even deeper over land (i.e., average echo tops at 8-10 km). Convection that does not produce anvil has average echo tops closer to 6 km. To further highlight the difference in convective echo

(a) Convective rain with anvil

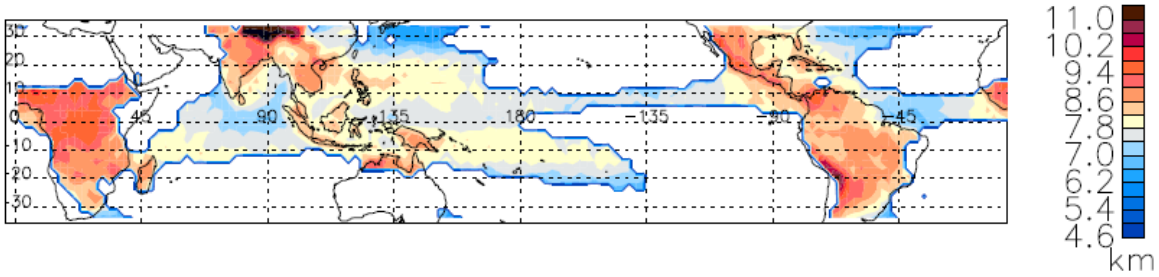

(b) Convective rain without anvil

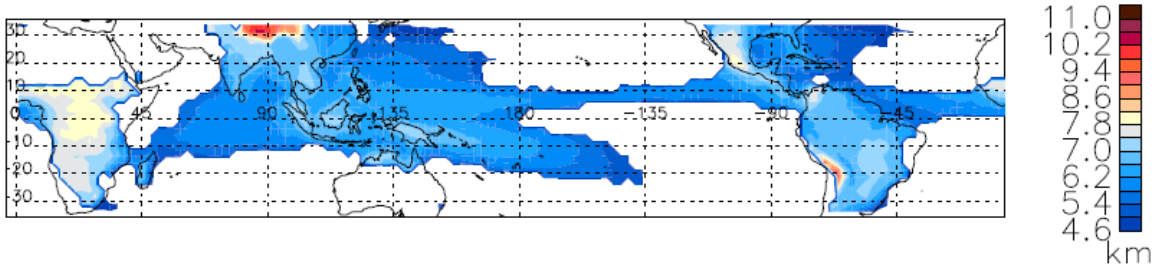

(c) Convective rain with anvil - Convective rain without anvil

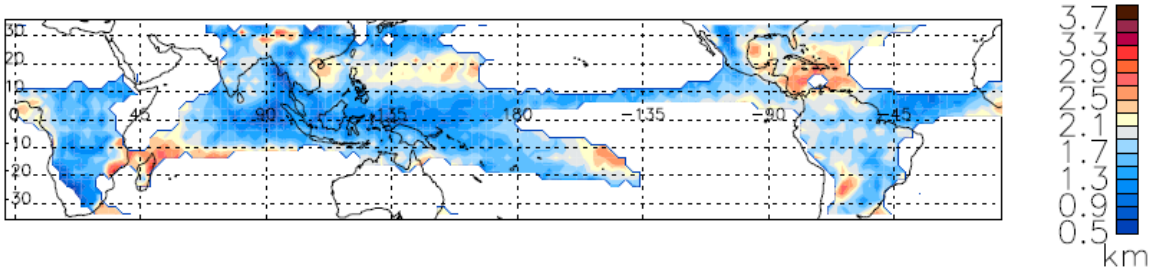

Figure 4. 1 Average echo top of convective rain based on 2.5˚ grid averages for 1998-2007 for (a) convective rain with anvil, (b) convective rain without anvil, and (c) the difference between (a) and (b).

tops when anvil is present and not, Fig. 4.2 shows the histogram of the daily mean grid values in each situation. When 20 dBZ convective echo tops reach 5 km, anvil is not that common, whereas at 6 km there is an equal chance for anvil to occur or not to occur. Anvil becomes much more likely once convective echo tops reach 7 km.

The difference between Figs. 4.1a and b (shown in Fig. 4.1c) indicates that convection that generates anvil is 1-3 km deeper than convection that does not. Regions where deep convection is prevalent, such as Africa, the West Pacific, and South America, show smaller echo top differences than regions where deep convection is less common, such as the western Indian Ocean, northwest tropical Pacific, and Caribbean. This result suggests that variations in the large-scale environment may play a more important role in anvil production variability in regions where convection regularly attains heights greater than 7 km. For regions where convection is less deep, variations in the depth of the convection and the large-scale environment likely contribute more equally to anvil generation variability.

Convective strength also appears to be associated with thick anvil production. As shown in Fig. 4.3, more intense convection tends to generate thick anvil. For example, the mean reflectivity at 2 km for convection that produces anvil is 34-35 dBZ over Africa (Fig. 4.3a), but is 32-33 dBZ for convection that does not (Fig. 4.3b). The differences over Africa are the largest in the tropics (Fig. 4.3c). In general, reflectivity differences between convection that does and does not produce anvil is closer to 1 dB. This relationship is further highlighted in the histograms in Fig. 4.4. When 32 dBZ is observed at 2 km height in a convective cell, the convection is equally likely to produce anvil as not; however, when 34 dBZ is observed, anvil is much more likely to occur. In addition,

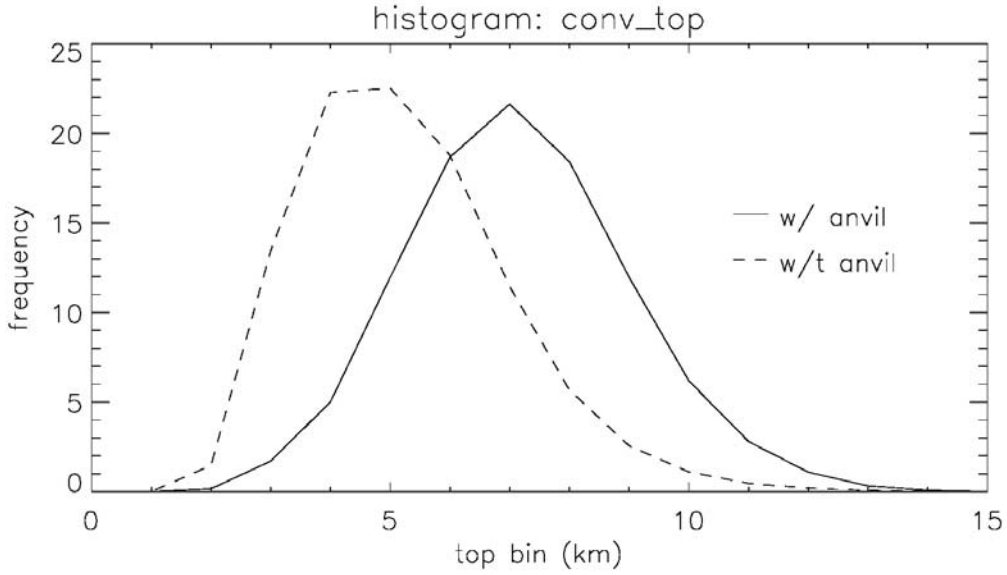

Figure 4. 2 Frequency distributions of daily grid average convective echo tops with and without anvil.

(a) Convective rain with anvil

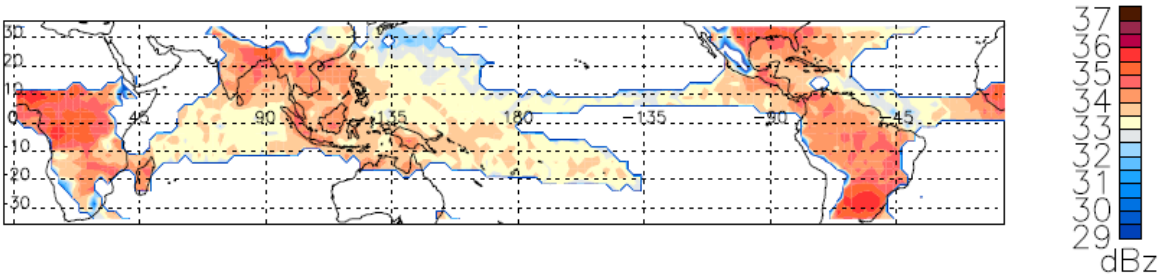

(b) Convective rain without anvil

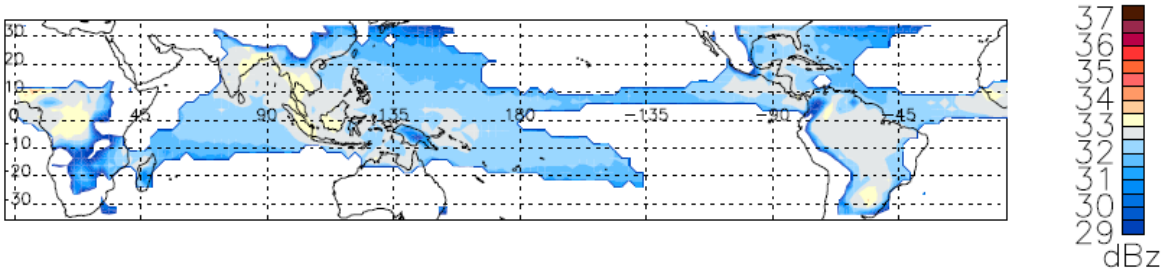

(c) Convective rain with anvil - Convective rain without anvil

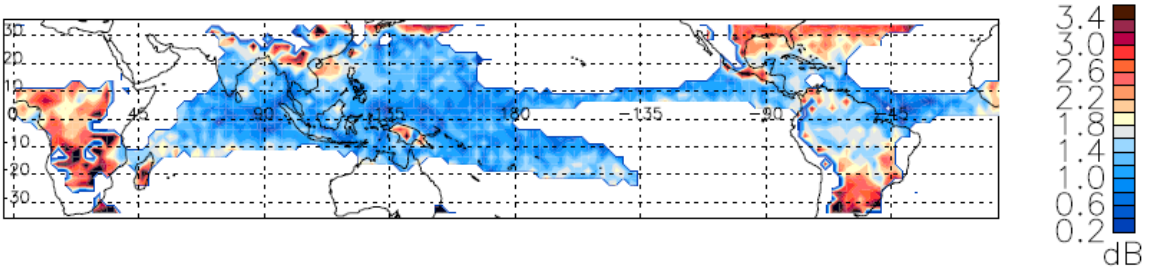

Figure 4. 3 Average reflectivity of convective rain at 2 km based on 2.5˚ grid averages for 1998-2007 for (a) convective rain with anvil, (b) convective rain without anvil, and (c) the difference between (a) and (b).

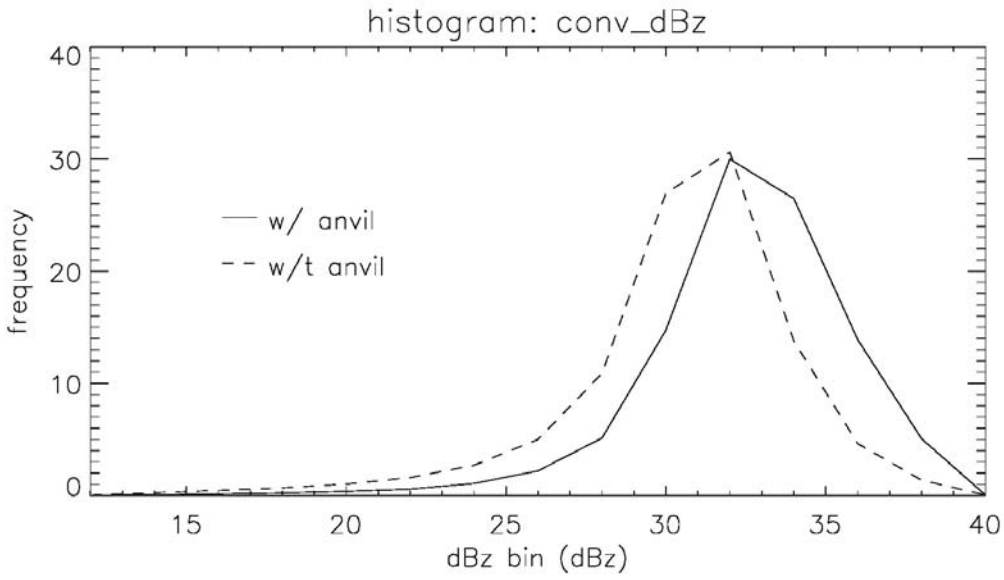

Figure 4. 4 Frequency distributions of daily grid average convective reflectivity at 2 km with and without anvil.

anvil-producing convection over land is 1-2 dB stronger than anvil-producing convection over ocean (Fig. 4.3a).

Since radar reflectivity is related to both hydrometeor size and number density, it is hard to say whether larger or more hydrometeors are produced at higher reflectivities. However, it is highly likely that stronger updrafts (especially over land) loft larger and/or more hydrometeors to higher heights, providing more fuel for the anvil region. It can also be speculated that updraft strength may change the hydrometeor density or size distribution in the anvil leading to changes in the anvil radiative heating profile.

The size of the convective rain area may also be linked to anvil generation. Anvil forms in the mature stage of tropical convective systems (Houze 1982, Machado and Rossow 1993); therefore, one would expect higher anvil areal coverage when more (or larger) convective cells are present. Anvil-producing convection (Fig. 4.5a) has conditional areal coverage ranging from 3-5%, whereas convection that is not associated with anvil (Fig. 4.5b) has conditional areal coverage closer to 2%. The difference between Figs. 4.5a and b (shown in Fig. 4.5c) is similar to the echo top difference map (Fig. 4.1c) in that larger differences are required to form anvil in regions where deep convection can be marginal or occur infrequently.

4.2 Convection's efficiency in generating thick anvil

Convection occurs in conjunction with thick anvil ~18% of the time across the tropics within the 2.5º daily grid boxes, but varies geographically (Fig. 4.6). Values are typically ~12% over ocean and 16~25% over land, but are even greater over Africa, the

(a) Convective rain with anvil

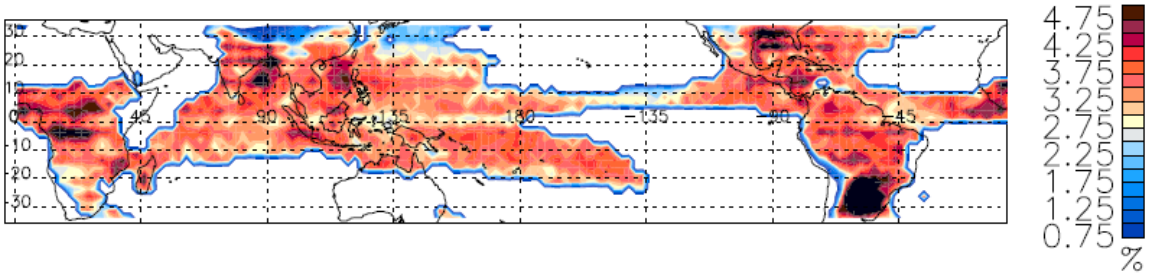

(b) Convective rain without anvil

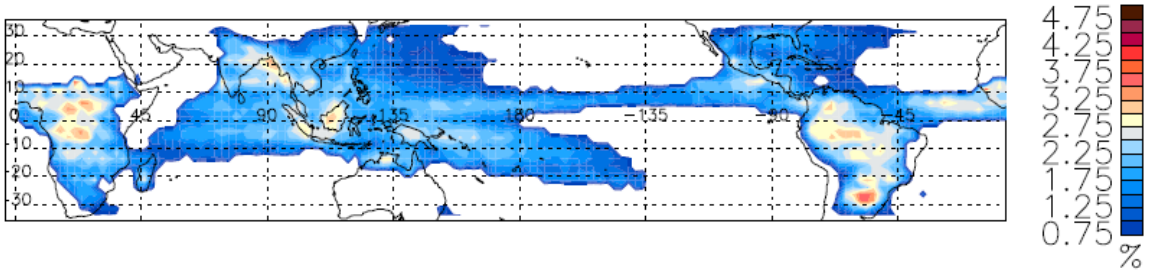

(c) Convective rain with anvil - Convective rain without anvil

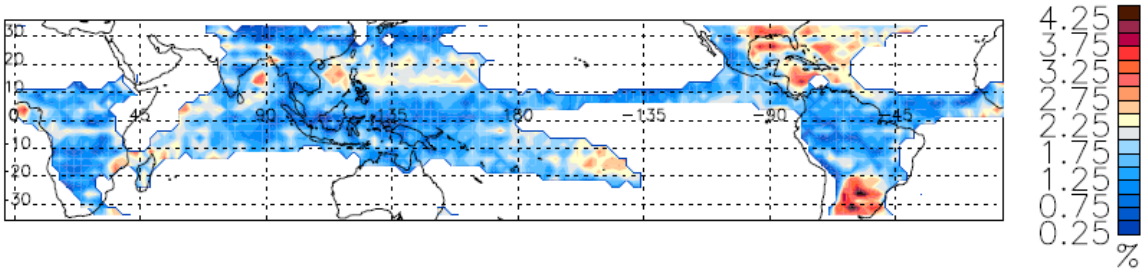

Figure 4. 5 Conditional areal coverage of convective rain based on 2.5˚ grid averages for 1998-2007 for (a) convective rain with anvil, (b) convective rain without anvil, and (c) the difference between (a) and (b).

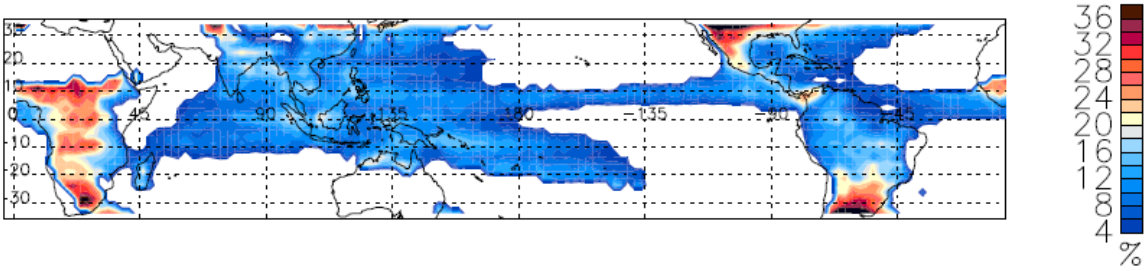

Figure 4. 6 Anvil-generating frequency of convective rain based on 2.5˚ grid averages. The anvil-generating frequency is defined as the number of days with both convective rain and anvil divided by the total number of days with convective rain during 1998-2007.

southern US and Mexico, and southern South America. Other land regions, such as the Maritime Continent and the Amazon basin, are notably closer to the tropics-wide mean.

Figure 4.7 shows the frequency distribution of anvil area as a function of convective rain area over Africa (land area in 30˚W-30˚E, 5˚S-15˚N), tropical South America (land area in 40˚W-90˚W, 15˚S-10˚N), and the West Pacific warm pool (ocean area in 90-180˚E, 15˚S-10˚N). Over Africa, the deep and intense mesoscale convective systems that generate anvil usually occur during the active monsoon period (Fortune 1980, Houze 1981, Thorncroft and Hodges 2001, Schumacher and Houze 2006, Futyan and Del Genio 2007, Cetrone and Houze 2009). In contrast, the seasonal variation of convection over the tropical ocean is weak. Tropical South America is recognized as a non-monsoon region. However, seasonal variability of convection and rainfall also exist in this region due to the seasonal shift of large-scale circulation (Wang and Fu 2002). During the wet season, the warm and moist environment (similar to the tropical ocean) provides favorable conditions for the formation of convection. Therefore, South America generally lies somewhere between Africa and the West Pacific in convective and anvil properties. With this in mind, Fig. 4.7 reveals the following signatures:

a) Land exhibits a wider spectrum of areal coverage than that over ocean. For example, Africa has convective rain areas ranging from 0 to 8% and anvil areas ranging from 0 to 4%, whereas the West Pacific is more tightly distributed with convective rain areas ranging from 1 to 6% and anvil areas ranging from 0 to 2.5%.

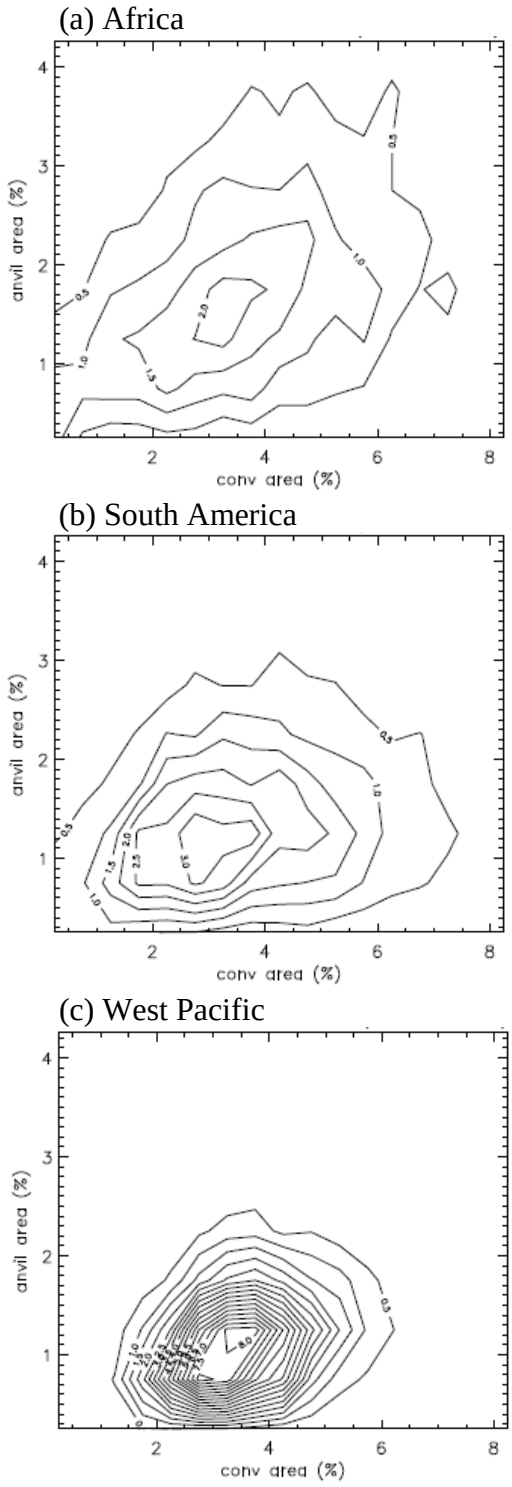

Figure 4. 7 Frequency distribution of the anvil areal coverage as a function of convective rain area (i.e., a two-dimensional histogram of convective rain and anvil area) for (a) Africa (land area in 30˚W-30˚E, 5˚S-15˚N), (b) South America (land area of 40-90˚W, 15˚S-10˚N), and (c) the West Pacific (ocean area within 90-180˚E, 15˚S-10˚N). Bin size is 0.5% for both convective rain and anvil area. The contour interval is 0.5%.

b) For the same convective rain area, more anvil is generated over land (~2.1/4 over Africa and ~1.5/4 over South America) than ocean (~1.2/4 over the West Pacific).

c) For both land and ocean, near-median convective rain coverage is associated with the most anvil generation. While it is easier to understand that smaller convective rain areas are related to less anvil generation, the reason for very large convective rain areas corresponding to less anvil generation is hard to determine. One possible reason is if the convective rain area is very large or highly organized, stratiform rain may form in preference to anvil (Schumacher and Houze 2006).

To further explore the relationship between stratiform rain and anvil production, Fig. 4.8 shows the areal coverage of thick anvil as function of stratiform rain area. Similar to the convective area plots, the spread of the frequency distribution decreases as one goes from Africa, to South America, to the West Pacific. However, the stratiform rain area median increases in that same order while the convective rain area median was stable between regions. In addition, the slope of the fit line is slightly positive over Africa, near zero over South America, and slightly negative over the West Pacific. Therefore, stratiform rain area does not appear to be a good predictor for anvil production. Schumacher and Houze (2006) had suggested that stratiform rain may grow at the expense of anvil in situations of low upper level wind shear and high low-level

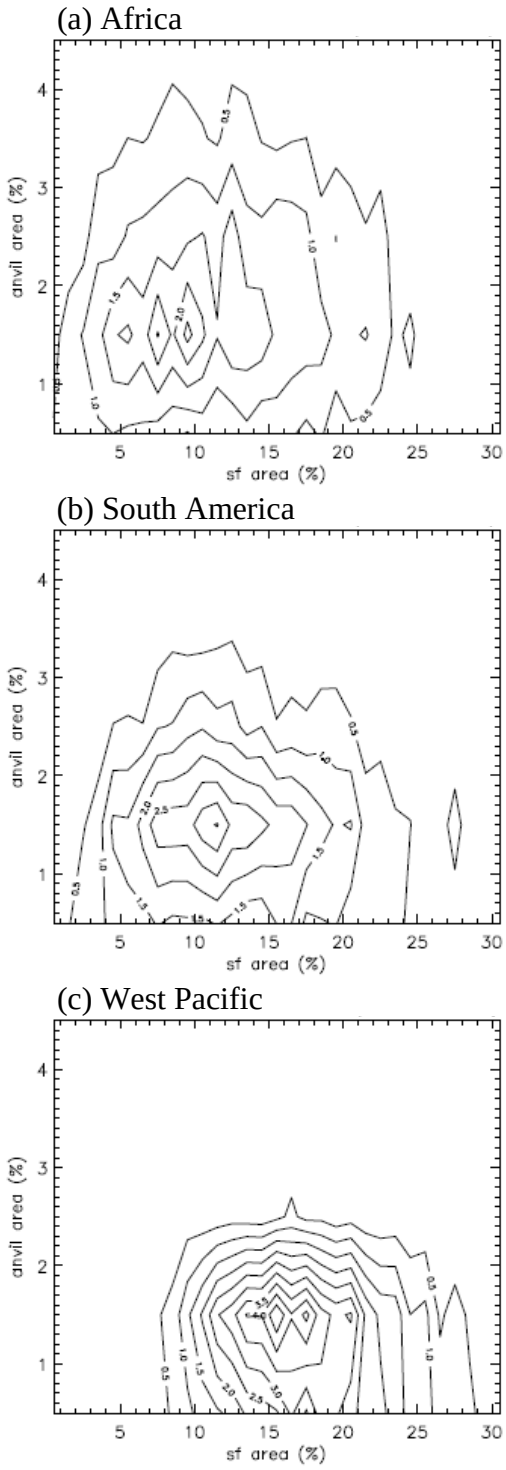

Figure 4. 8 The same as Fig. 4.7, but for stratiform rain area.

humidity, but this argument would only hold over the West Pacific based on these statistics.

4.3 Effect of the large-scale environment on anvil production

In tropical convective systems, stratiform precipitation accounts for a large fraction of total rain (Schumacher and Houze 2003) and using the C-POL observations from Darwin, Australia, Frederick and Schumacher (2008) showed that anvil typically formed after stratiform rain area peaked. In addition, upper level shear can be a factor in the formation of stratiform rain (Houze 1993, 1997). Therefore, this study compares the zonal wind profile during situations when stratiform rain and thick anvil coexist and when only stratiform rain occurs to differentiate the impact of upper level shear on the formation and maintenance of stratiform rain and anvil.

Figure 4.9a shows the zonal wind profile under the situation of no stratiform rain present, stratiform rain without anvil and stratiform rain with anvil over Africa, the West Pacific warm pool, and South America for 1998-2007 based on daily National Center for Environmental Prediction (NCEP) reanalysis data. The zonal wind over tropical Africa shows strengthening of the near surface westerlies and upper level easterlies when stratiform rain is present and even stronger reinforcement of the wind when stratiform rain and anvil coexist. In fact, Central and West Africa is under the influence of three circulations at different heights:

a) African Easterly Jet (AEJ): a prominent mid-tropospheric zonal jet resulting from strong meridional soil moisture gradients (Burpee 1972, Cook 1999)**.** The AEJ is prominent over Africa year-round at approximately 600-700 hPa.

b) Tropical Easterly Jet (TEJ): a prominent upper level jet at about 200 hPa. Since the TEJ originates over the Tibetan Plateau, it becomes most pronounced during boreal summer and extends from Southeast Asia to Africa.

c) Monsoonal flow: occurs near the surface of the earth due to the differential heating of ocean and land, which is featured as the increase of westerly winds during the wet season.

Schumacher and Houze (2006) speculated that strengthening of the TEJ over Africa favors the formation of stratiform rain. Further strengthening of the TEJ may then enhance the detrainment of hydrometeors from the stratiform rain region to form anvil. As shown in Fig. 4.9a, enhancement of the upper level TEJ appears to positively impact the formation of anvil over Africa.

The West Pacific warm pool experiences weak tropical easterlies through all levels. The zonal wind profile shows the weakening of the easterlies (or strengthening of the westerlies) below 300 hPa and strengthening of the easterlies above. However, compared to tropical Africa, the difference between the anvil and no-anvil situation is small. Therefore it appears that upper level shear plays less of a role in anvil production over the West Pacific. The MCSs over this region are larger and live longer than over many other tropical regions (Chen et al. 1996), such that convective rain area coverage may be more relevant.

South America is generally influenced by low-level easterly winds and weak upper level westerly winds; opposite of Africa during the monsoon season. However, the change of zonal wind shear is in the same sense of Africa, such that the zonal wind

profile difference (i.e., enhancement of the easterlies) between 500-200 hPa appears to be conducive to anvil production.

Figure 4.9b is similar to Fig. 4.9a, but shows the relative humidity profile for each region. Over Africa, the entire atmospheric column is more humid by ~6% when anvil is present, while humidity increases are close to zero at low levels and increase to 6% above 600 hPa over the West Pacific and South America in the presence of anvil. It is unclear whether this increase is the result of anvil moistening the atmosphere or the more humid environment assisting in anvil generation. However, Sobel et al. (2004) suggested that stratiform rain regions moisten the mid and upper troposphere based on lag correlations over Kwajalein in the central-west Pacific and the PR-observed stratiform rain regions are larger over these regions when anvil is present (14% vs. 5%). Thus, the more robust stratiform rain regions may account for the moister environment when anvil is present, or anvil may similarly act to moisten the mid and upper troposphere.

Based on the results from this section, the generation of anvil in the presence of stratiform rain may be separated into two stages. In the first stage, a certain amount of upper level wind shear enhances hydrometeor detrainment from deep convection, thus feeding and increasing the stratiform rain area. The environmental humidity correspondingly increases in the mid and upper troposphere. When the wind shear strengthens further, the top part of the stratiform rain area is advected away to form anvil. The geographical variation of anvil vertical extent (i.e., higher and thicker anvil over land) implies that there may be a deeper layer of upper level wind shear over land through which deep convection extends and from which material is blown off to form

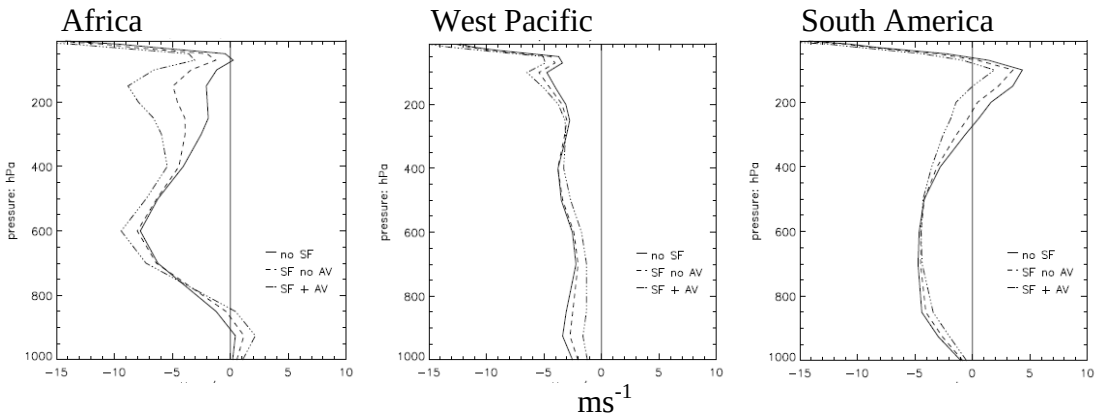

(a) Zonal Wind

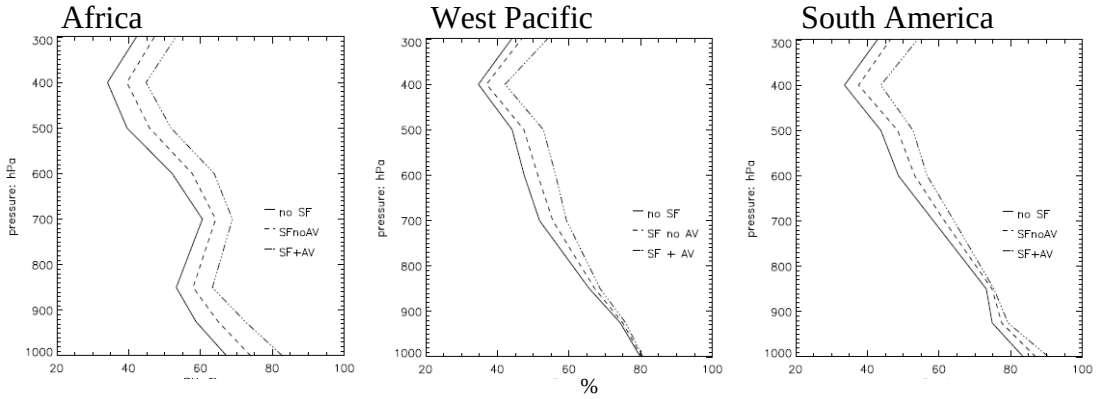

(b) Relative Humidity

Figure 4. 9 (a) zonal wind and (b) relative humidity profiles for situations when no stratiform rain is present, stratiform rain without anvil and stratiform rain with anvil over Africa, the West Pacific and South America based on daily NCEP reanalysis fields for 1998-2007.

anvil. Over ocean, the lower and less thick anvil suggests upper level wind shear is less effective in advecting hydrometeors from the less deep parent convection.

CHAPTER V

ANVIL RADIATIVE HEATING

The traditional method of calculating cloud radiative heating is to use a radiative transfer model; however, this method is computationally intensive and not feasible for the 10-year TRMM PR data set. Thus, this study uses a 'look-up table' based on high-fidelity MMCR radiative heating calculations to estimate the tropics-wide TRMM PR anvil radiative heating. This chapter discusses this approach and possible uncertainties in the heating estimates. In addition, the CloudSat radiative heating product (representing a shorter time series and smaller spatial coverage than the TRMM PR) is used to assess the TRMM PR retrieval.

5.1 Radiative heating estimates

a. Cloud water content of PR anvil

Cloud radiative heating is largely determined by cloud optical depth, which is primarily determined by cloud water content (i.e., ice water content [IWC] plus liquid water content [LWC]). The regression between equivalent radar reflectivity *Ze* and the CWC of the cloud (i.e., a *Ze*-I or LWC relation) has been widely used to parameterize CWC for a given radar reflectivity (Gunn and Marshall 1958, Brown and Braham 1963, Heymsfield and Palmer 1986, Matrosov 1999, Black 1990, Sassen and Liao 1996, Fox and Illingworth 1997, Sassen et al. 2002, Heymsfield et al. 2003, Jensen and Del Genio 2003). The *Ze*-CWC relation varies from cloud to cloud (Black 1990) and radar to radar, primarily due to the different mass distribution with cloud particle size.

This study utilizes the following regression equations: $IWC=0.01Ze^{0.66}$, which was derived from a least square fit of airborne radar and aircraft observations of a convective region of Hurricane Irene (Black 1990), and $LWC=0.46Ze^{0.2}$, which was derived from radar and lidar observations of stratocumulus and in-situ particle probe instruments (Baedi et al. 2000). For both relations, it is assumed that the cloud hydrometeors in the anvil satisfy a lognormal size distribution (Ackerman et al. 1988, Jensen and Del Genio 2003) and for the *Ze*-LWC relation, it is assumed that the cloud particle size is much smaller than the radar wavelength so that Rayleigh scattering is satisfied (Jensen and Del Genio 2003). Using these relations, TRMM PR tropical anvil CWCs usually range from 0.2~1.4 gm^{-3}, which is reasonable compared to in-situ measurements of convective cloud (Liou 1992).

It is also possible that mixed phase hydrometeors exist in anvil. There are several definitions of the mixed phase layer, usually from the melting level (0 °C) to -10, -20, or -30 °C (Yeh et al. 1990). In this study, 5-7 km is chosen to represent the mixed phase layer. That is, only ice is assumed to occur above 7 km and only water below 5 km. Similar to Wu and Weinman (1984), in the transition layer (i.e., 5-7 km) cloud water content is defined as:

$$CWC = (\frac{z-5}{2})LWC_{5km} + (\frac{7-z}{2})IWC_{7km} \qquad 5 \le z \le 7km$$

The use of the above equation removes any discontinuities in the CWC profile resulting from the assumption that only water or ice hydrometeors are present.

As discussed in chapter II, the low sensitivity of the PR limits its ability to detect small ice hydrometeors near cloud top. Therefore, an echo top correction is applied to each anvil CWC profile. Across the tropics, PR underestimated echo top by 1-10 km with

an average 5 km compared to CloudSat. Sensitivity tests were performed to determine the best echo-top correction. This study either randomly added a Δh, which ranged from 1 to 10 km, or a fixed 5 km on the original PR CWC profile and then linearly decreased the top CWC value to zero. The resulting average anvil radiative heating profile showed little sensitivity to the echo-top correction employed. Therefore, the PR anvil CWC profile is simply modified by adding 5 km of linearly decreasing CWC to the original profile.

b. MMCR radiative heating

Major goals of DOE ARM are to improve the understanding of cloud-radiation feedbacks in the atmosphere and to promote the performance of climate models. Toward these goals, ARM set up several long-term measurement sites to represent a broad range of environmental conditions. The TWP sites at Manus (2.06°S, 147.42°E), Nauru (0.52°S, 166.92°E), and Darwin (12.42°S, 130.89°E) provide high vertical and temporal resolution cloud properties from a suite of active and passive remote sensing instruments, including the MMCR (McFarlane et al. 2005, Mather et al. 2007). These cloud properties and the necessary atmospheric state parameters can be used to calculate radiative heating profiles. In addition, cloud types passing over the TWP sites are typical of the wider tropical western Pacific region (Jakob and Tselioudis 2003). Therefore, this study assumes the cloud radiative heating calculations at the TWP sites are representative of the broader tropics and extrapolate them to TRMM PR anvil.

The data used in this study are the CWC and broad band heating profiles from Manus (hereafter called the MMCR dataset) during April 2000 – September 2006 (data from 2001 is not available, 1046 days in total) with ~45 m vertical resolution and 5 min temporal resolution. Shorter datasets from the other TWP sites were also analyzed, but

did not change results using the longer dataset from Manus. Once the CWC for each TRMM PR anvil is obtained (Fig. 5.1a), a least squares technique is used to find a matching CWC profile in the MMCR dataset (Fig. 5.1b). The corresponding MMCR heating profile for the matched CWC profile with the mean clear-sky component subtracted is assumed to be the heating profile of the PR anvil (Fig. 5.1c).

The advantage of this approach is that it overcomes the limitations of the PR's sensitivity and the lack of a long time series and poor spatial coverage of the MMCRs. This methodology is less accurate than explicit radiative transfer calculations, but is much more efficient for large datasets (such as from the 10-year PR record) and maintains the primary features of the high-quality MMCR heating profiles. It should be noted that while the CloudSat CPR provides high sensitivity observations and tropics-wide coverage, its relatively short time in space compared to the PR and its nadir-only view means that it will have to be in orbit many more years before a comprehensive anvil climatology can be produced.

c. Uncertainties in extrapolating MMCR radiative heating to TRMM PR anvil

1) Diurnal variation of solar radiative heating

Diurnal variations in solar heating are significant; however, the matched heating profile from the MMCR dataset may be from any time of the day. Therefore, the chosen shortwave heating profile is normalized to take into account diurnal variability. First, the temporal mean diurnal variation of the column-integrated shortwave heating was calculated (Fig. 5.2). From this distribution, a weighting parameter for shortwave heating

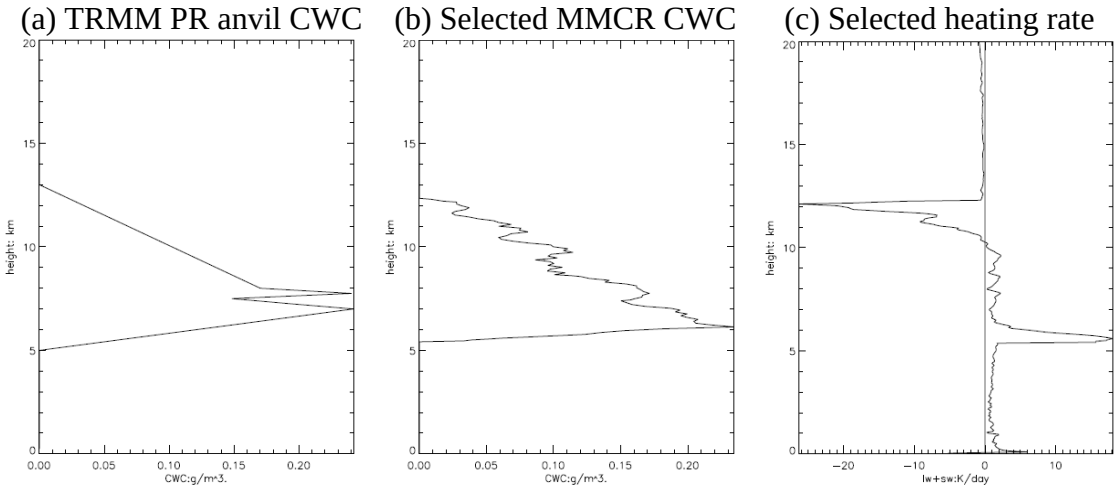

Figure 5. 1 Example of (a) a TRMM PR anvil CWC profile, (b) the best match MMCR CWC profile, and (c) the corresponding MMCR net radiative heating rate.

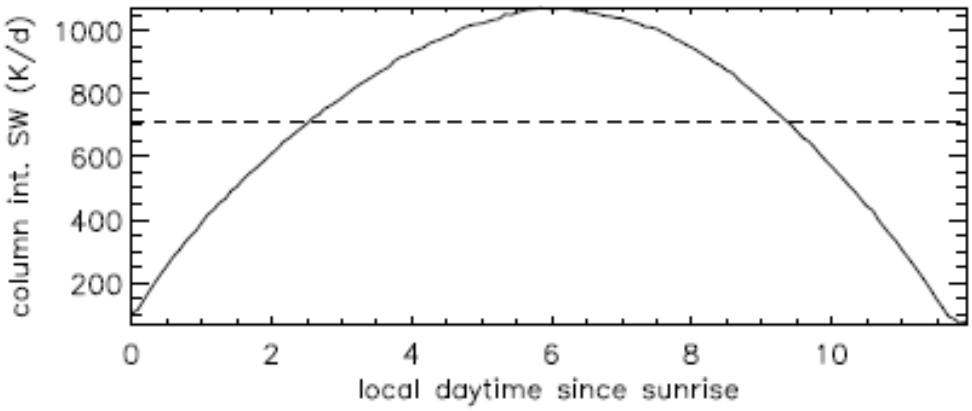

Figure 5. 2 Diurnal variation of column integral of solar heating rate in MMCR data at Manus.

at each time was obtained, i.e., $w(i) = swhr(i) / \overline{swhr}$, where $\overline{swhr}$ is the temporal mean shortwave heating rate. This relation is applied to the shortwave heating profile chosen at any time from the MMCR, that is, $swhr(i)$ is divided by $w(i)$ to obtain the approximate daily mean shortwave heating rate. The longwave heating rate does not show significant diurnal variability so no weighting is done. In addition, seasonal and geographical variations in solar radiative heating are ignored since these variations are relatively small in the tropics.

2) Multilayer cloud

Up to this point, it has been assumed that there is no cloud unobservable by the PR above or below the anvil. MMCRs have the ability to detect multilayer clouds (Naud et al. 2005) if the cloud is not too thin or high (Mather et al. 2007). To ascertain potential effects of multilayer cloud on the anvil radiative heating retrieval, this study analyzes how often an additional thin cloud layer occurred above anvil and its contribution to radiative heating using the MMCR at Manus. If cloud occurs under the anvil, it is probably precipitation debris or shallow convection, which the PR is usually able to see.

The retrieved PR CWC is always greater than 0.1 g m^{-3}, so this is the maximum value a multilayer cloud is allowed to have in the MMCR analysis. Based on the multiyear MMCR observations, an additional cloud layer occurs above ice anvil 9% of the time and above mixed anvil 21% of the time. Figure 5.3 shows that the additional cloud layer reduces the radiative cooling aloft for both anvil types by about 1 K d^{-1}. In addition, radiative heating between 7 and 9 km is reduced by less than 0.5 K d^{-1}. In the PR anvil radiative heating estimation discussed in the next section, the multilayer cloud

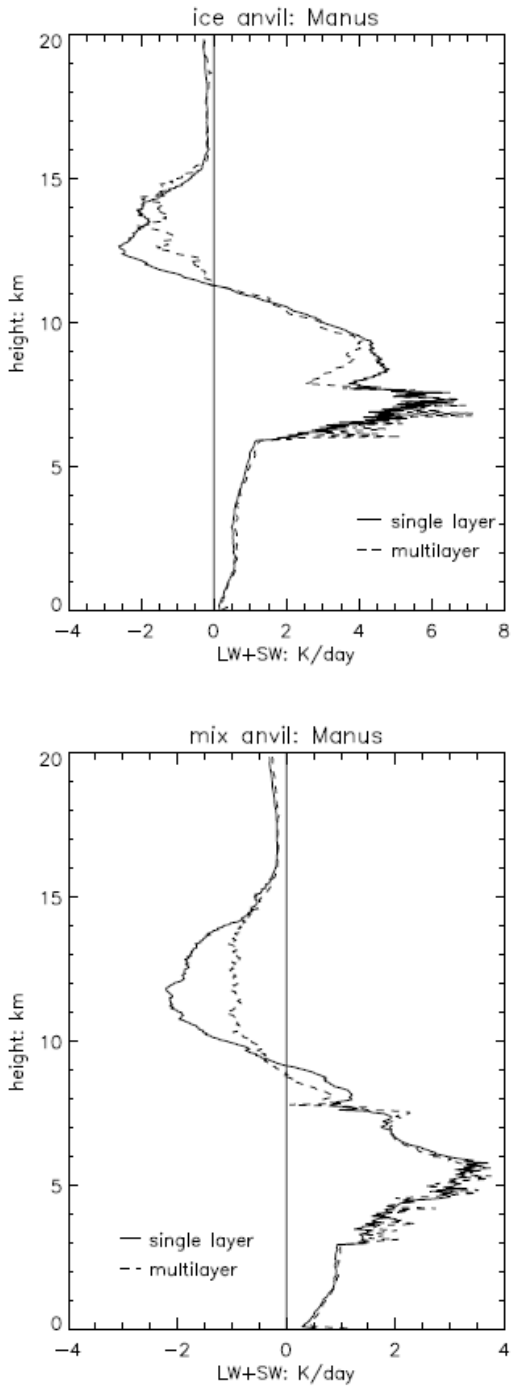

Figure 5. 3 MMCR anvil radiative heating profiles for ice (top) and mixed (bottom) anvil types with and without the presence of another cloud layer above the anvil.

impact is ignored. However, this comparison indicates that if there is an extra cloud layer above the thick anvil, the cooling effect can be weakened to some degree. Also note that the MMCR profiles in Fig. 5.3 include heating rates from all reflectivity columns that meet the PR anvil geometric definitions. Some of this 'anvil' is not optically thick, in contrast to the PR anvil, so the MMCR heating profiles will not necessarily be directlycomparable to the TRMM PR heating profiles in the next section.

5.2 TRMM PR anvil radiative heating

Figure 5.4 shows the net radiative heating profile of TRMM PR ice anvil, mixed anvil and total anvil across the tropics for 1998 to 2007. Ice anvil has a heating maximum of 9 K d^{-1} from 7.5 to 9 km and cooling maximum of -6 K d^{-1} between 12 and 14 km, while mixed anvil has heating maximum of 7 K d^{-1} near 6 km and cooling maximum of -5 K d^{-1} at 12 km. These results are generally consistent with Fig. 9 in Webster and Stephens (1980) in that the heating maxima for both anvil types result from longwave heating at cloud base, while the cooling maxima result from longwave cooling moderated by shortwave heating at cloud top. However, the PR mixed anvil radiative heating profile shows that little heating or cooling occurs throughout the middle of the cloud because of its high optical thickness, which is consistent with Ackerman et al. (1988) and Machado and Rossow (1993) but is in contrast to Webster and Stephens (1980) who (likely erroneously) indicated a linear decrease from cloud base to cloud top. Ice anvil is usually physically and optically thinner than mixed anvil so does not show a layer of near zero heating between cloud base and cloud top. The column-integrated radiative effect of ice anvil is net heating while the heating and cooling in mixed anvil nearly cancel each other.

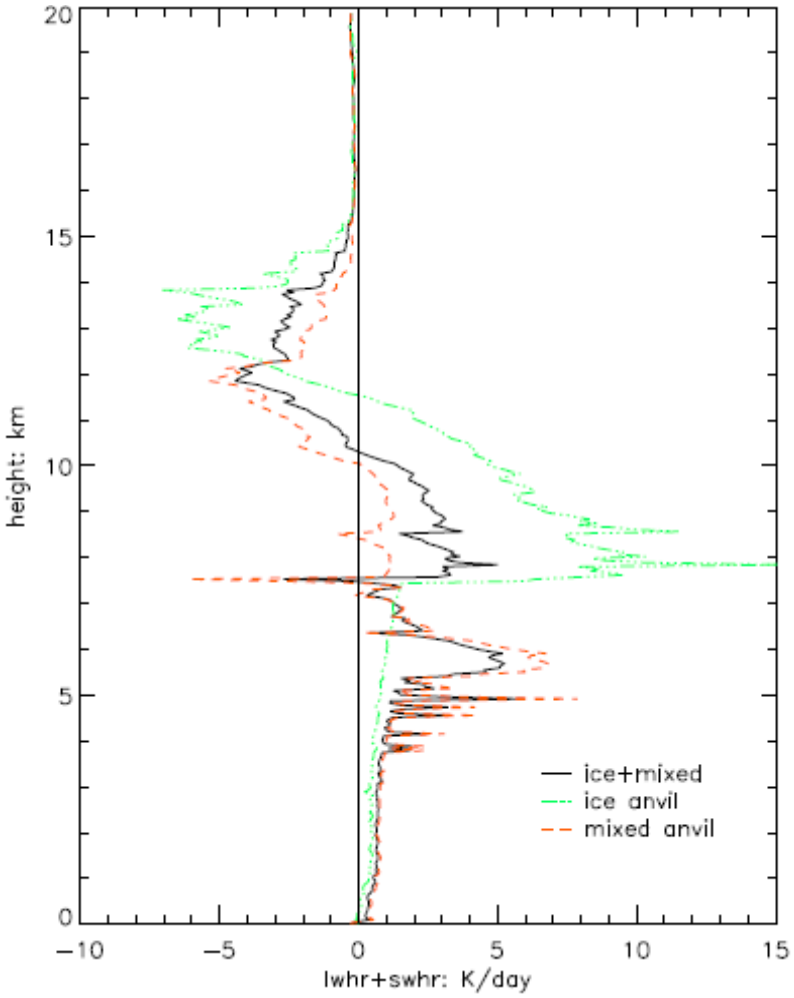

Figure 5. 4 TRMM PR average anvil radiative heating profiles from 20°S–20°N during 1998-2007.

The resulting total anvil radiative heating profile indicates heating from the surface to 10 km with a maximum heating of 5 K d^{-1} just below 6 km and a secondary maximum of 3 K d^{-1} between 7.5 and 9 km. Cooling occurs from 10 to 15 km with a maximum cooling of -5 K d^{-1} at 12 km. Machado and Rossow (1993) calculated radiative heating rates of tropical mesoscale anvil (i.e., thick anvil and cirrus with bases higher than 600 hPa) based on eight months of ISCCP data and a radiative transfer model and the resulting net heating profile (their Fig. 16c) showed a similar structure to the TRMM PR retrieval, even though our study did not include the radiative effects of stratiform rain or cirrus. Further evaluation of the TRMM PR radiative heating retrieval through comparison with the CloudSat CPR heating product will be presented in next section.

To investigate regional differences in anvil radiative heating, Fig. 5.5 shows the vertical cross section of the PR-derived anvil radiative heating along 10°N assuming 100% anvil coverage. Observed anvil coverage will be taken into account in chapter VI. Enhancements in the heating profile over Africa (0-45°E) and South America (70°W) are evident, which is consistent with the results in chapter III that showed thick that anvil over these tropical land regions is deeper than over the tropical oceans.

5.3 CloudSat anvil radiative heating

This study uses CloudSat CPR retrievals to evaluate the TRMM PR anvil radiative heating profiles obtained from the look-up table method. Radiative heating profiles and related cloud properties of thick anvil observed by the CloudSat CPR were obtained from CloudSat products 2B-FLXHR, 2B-GEOPROF, and 2B-CWC-RO. Using Riley and Mapes's (2009) cloud types as a basis, CloudSat thick anvil was defined as cloud with a base between 3 and 8 km, a thickness larger than 5 km, and a maximum

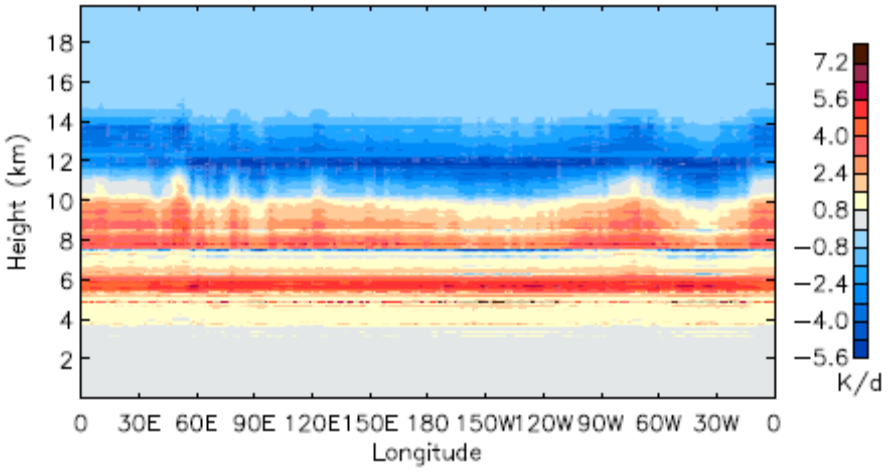

Figure 5. 5 Longitude-height cross section of 10–year mean TRMM PR anvil radiative heating along 10°N assuming 100% anvil coverage.

CWC greater than 0.2 g m^{-3}. Only clouds with a cloud mask value greater than 20 and reflectivity values between -25 and 30 dBZ were considered. In addition, only single layer clouds were analyzed. Figure 5.6 shows example CloudSat thick anvils (denoted by red crosses at the bottom of each image) based on the above criteria. The radar echo is generally attached to deep convection, but is occasionally separate from the parent system. However, the radiative heating profiles in both situations show similar characteristics. Sensitivity tests also showed that the tropics-wide mean anvil radiative heating profile of the CloudSat CPR is not sensitive to seasonal variation, so for convenience, this study used only 500 orbits (around one month) starting from 1 August 2006 for the analysis below.

Figure 5.7 compares the tropics-wide average TRMM PR and CloudSat anvil radiative heating profiles. The PR profile (Fig. 5.7a, reproduced from Fig. 5.4) generally resembles the CloudSat profile except that the CloudSat profile (Fig. 5.7b, solid line) is about 1 km higher and has smaller absolute magnitudes (by ~1 K d^{-1}). The difference in the profiles is primarily due to the sensitivity of the radars and the retrieval of the cloud water content. CloudSat anvil CWC is usually smaller than PR anvil CWC, which leads to a smaller heating rate. In addition, the deeper anvil heating profile in CloudSat indicates that uncertainties may still exist in the PR anvil top correction. However, this comparison suggests that the PR anvil heating retrieval using a look-up table method is reasonable.

Figure 5.7b also shows the average CloudSat anvil radiative heating profile subset for when the PR also saw anvil based on data from the 2D-CLOUDSAT-TRMM product during 1 August 2006-31 December 2008, which includes coincident CloudSat/TRMM

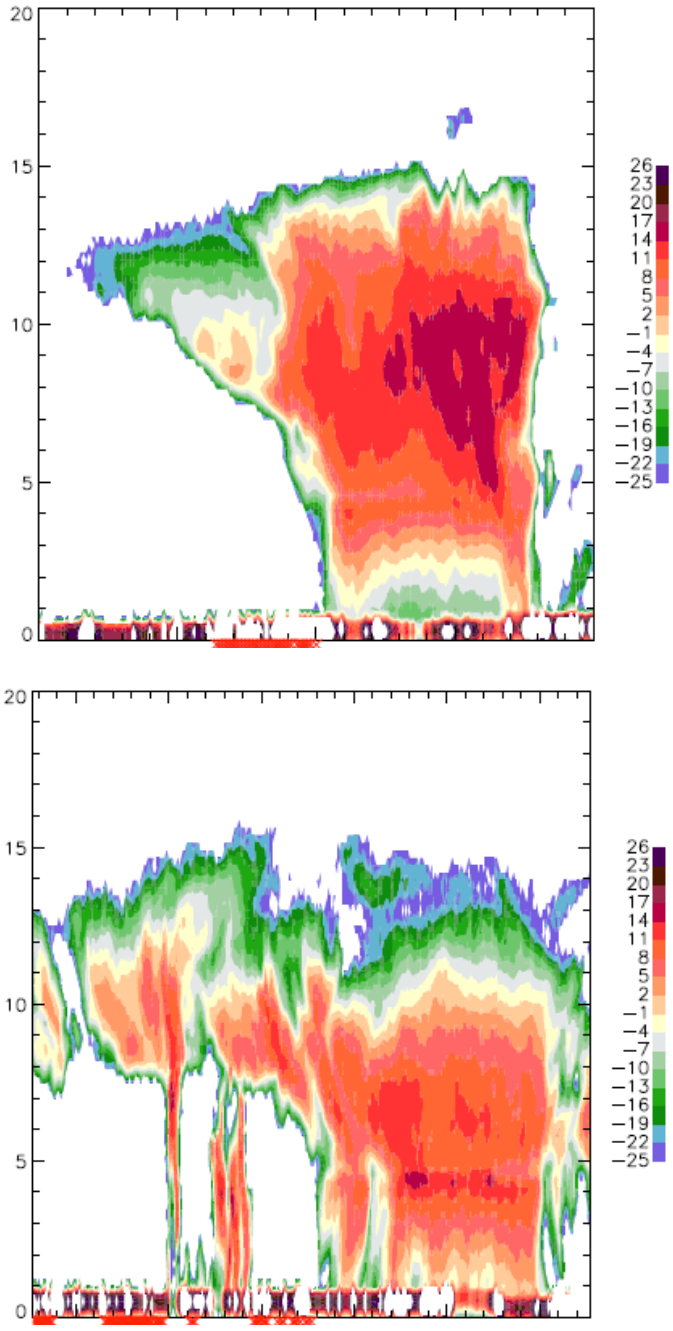

Figure 5. 6 Two examples of CloudSat anvil. CloudSat-defined anvil regions are marked by red crosses at the bottom of each image. The x-axis is the along track index and the y-axis is height (km). The color bar is reflectivity in dBZ.

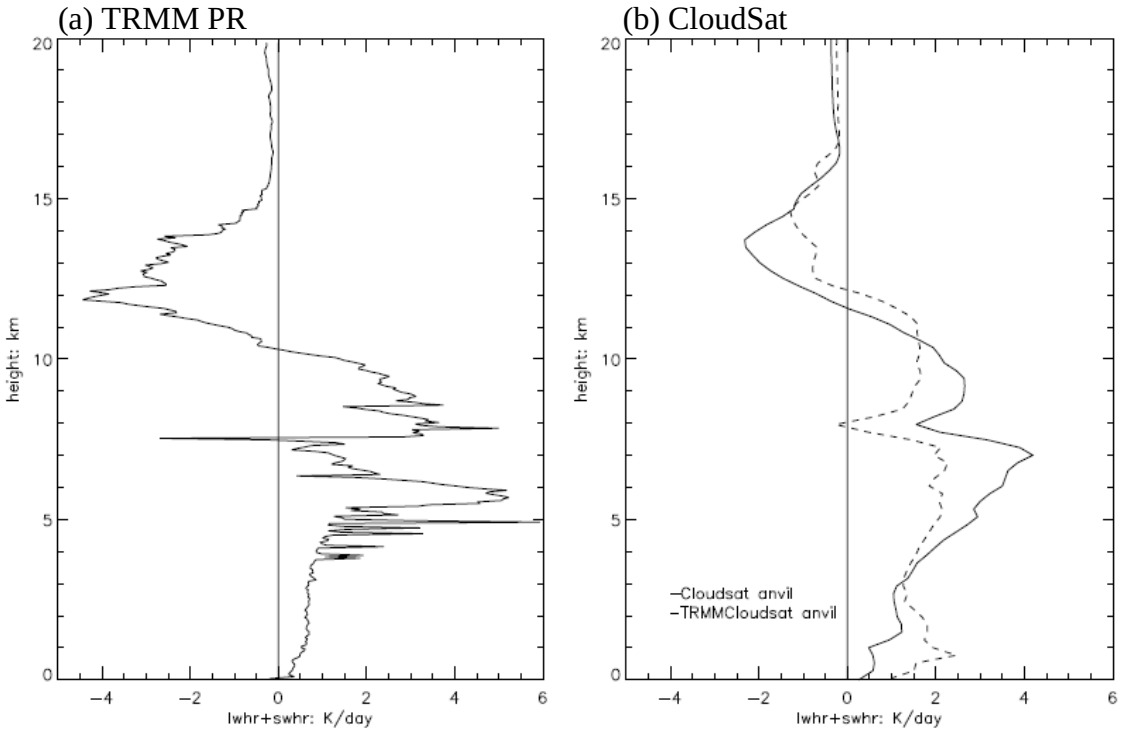

Figure 5. 7 (a) TRMM PR mean anvil radiative heating profile reproduced from Fig. 5.4 and (b) CloudSat mean anvil radiative heating profile (solid line) and the TRMM-subset CloudSat mean anvil radiative heating profile (dashed line).

overpass observations. Compared to the PR and CloudSat profiles, the TRMM-subset CloudSat profile shows thicker heating and cooling layers but smaller heating and cooling maxima. In addition, there is more low-level heating in the TRMM-subset CloudSat profile because CloudSat sometimes sees echo bases lower than 3 km when the TRMM PR says anvil is present.

5.4 Cirrus radiative heating

While radiative heating associated with cirrus is not the focus of this study, this section provides a preliminary assessment of the cirrus cloud contribution to tropical diabatic heating profiles, especially since cirrus radiative heating may also play a role in regulating the large-scale circulation. Cirrus (both thin and subvisible) is abundant over the tropics and has significant impacts on troposphere-to-stratosphere transport and the atmospheric radiation budget (Sherwood 1999, Liou 2002, Comstock and Ackerman 2002, Corti et al. 2006). Since the TRMM PR cannot sense cirrus, this study used MMCR data to estimate the radiative heating rate of cirrus. Cirrus is identified as cloud with a base higher than 7 km and a top higher than 9 km based on Riley and Mapes (2009). To isolate the cirrus heating profile, only single layer cirrus is considered in this study.

Figure 5.8 indicates that cirrus radiative heating is smaller than thick anvil radiative heating (the maximum heating is about 1.5 K d^{-1}). In addition, the maximum heating occurs between 9 and 11 km instead of at 8 km and the cirrus profile does not show much cooling aloft.

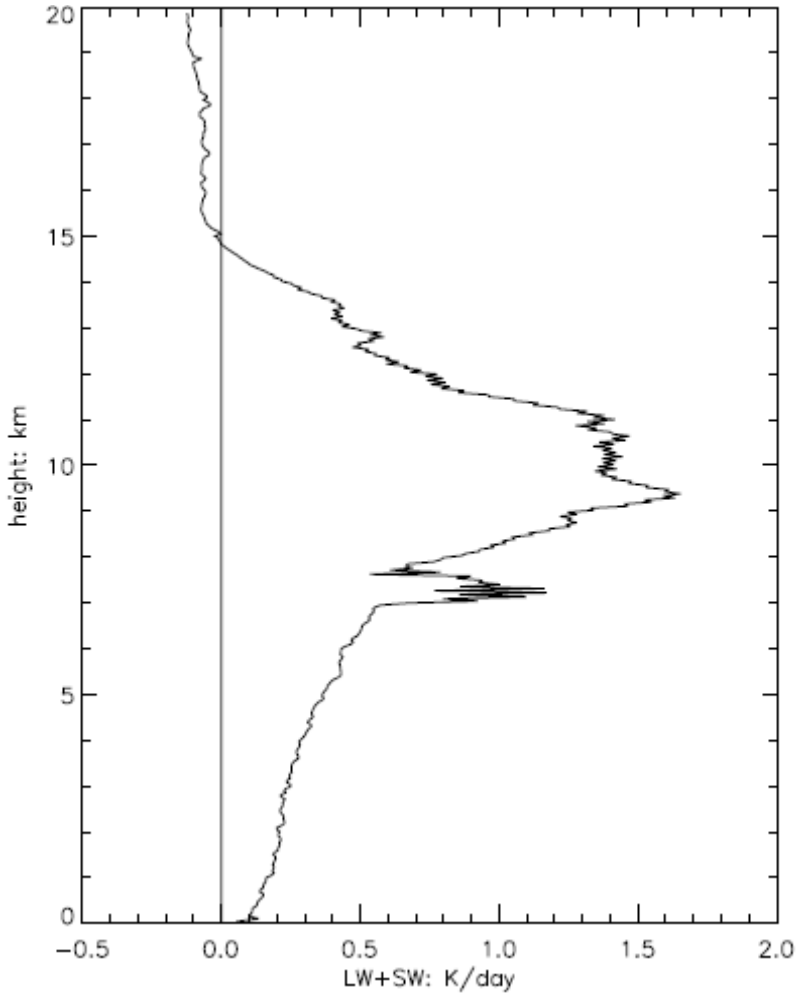

Figure 5. 8 MMCR cirrus radiative heating profile at Manus.

CHAPTER VI

IMPLICATIONS FOR THE LARGE-SCALE CIRCULATION

This chapter investigates the significance of the anvil radiative heating and the cloud radiative forcing associated with other cloud types on the large-scale tropical circulation by using an idealized climate model. It also discusses how cloud radiative heating modifies the circulation response to latent heating associated with tropical convective systems. The final aim of this doctoral work is to more fully understand the relationship between diabatic heating associated with convective cloud systems and the large-scale tropical circulation.

6.1 Model

This study uses an idealized version of the NCAR CAM3 to investigate the response of the large-scale circulation to tropical CRF. CAM3 was run at T85 with a horizontal resolution of ~1.4°×1.4°, 26 vertical levels, and a rigid lid at about 3 hPa. The boundary conditions and physical processes of the model were replaced with linear damping of temperature and wind perturbations towards a prescribed basic state to isolate the radiative heating impact. In addition, to obtain the zonally asymmetric large-scale response to the applied forcing and to prevent interaction between the zonally asymmetric response and mean flow, the zonal mean of the dynamical response (temperature, wind, surface pressure, divergence, and vorticity) was not allowed to change with time and topography and water vapor was removed from the model. Under these conditions, the model provides a non-linear, zonally asymmetric, quasi-steady state atmospheric response with respect to the magnitude of input TRMM PR heating. The same processing

and choice of coefficients for Newtonian cooling and Rayleigh friction can be found in Schumacher et al. (2004). All of the following numerical experiments are based on a motionless basic state. The thermal profile bears the tropical mean static stability.

6.2 Dynamic response assuming 100% anvil areal coverage

The Walker Circulation is driven by intense heating associated with deep convective systems over Africa, the Maritime Continent, and South America. These regions all show enhanced anvil radiative heating (see Fig. 5.5); therefore, the impact on the Walker Circulation is highly relevant when assessing the dynamical effect of anvil radiative forcing. To isolate the dynamical impact over regions where anvil radiative forcing is more intense, we forced the model with anvil radiative heating located over Africa (20°S–20°N, land only), the West Pacific (90°–180°E), and South America (20°S–10°N, land only), in addition to anvil radiative heating across the entire tropics. The input forcing in each case is the PR-derived three-dimensional anvil radiative forcing assuming each region is covered 100% with anvil. Zonal mass flux is used to analyze the dynamical response of anvil radiative forcing in a vertical plane. The zonal mass flux (Newell et al. 1974) is defined as:

$$M(p) = \frac{a\Delta\Phi}{g}\int_{p_0}^{p}\langle u'\rangle dp$$

where a is the radius of the earth and $\Delta\Phi$ is the width of the latitude strip (centered at the equator) in which the zonal mass flux is calculated. In this case, $\Delta\Phi$ =20°. $\langle u'\rangle$ is the 10°S–10°N averaged eddy zonal wind. Since the divergence of meridional wind is smaller than the zonal mass flux, if this term is ignored, mass is conserved in the longitude-height plane. Then the latitude-strip mean zonal mass flux can be regarded as

the approximate streamfunction. For the resting basic state, the model usually reaches equilibrium after two weeks (similar to Schumacher et al. 2004). To obtain a more stable solution, results from the 20th day are used to represent the steady-state solution.

As shown in Fig. 6.1a-c, all imposed local heating resulted in anticyclonic (positive zonal mass flux) zonal circulation to the right of the heating and cyclonic (negative zonal mass flux) circulation to the left of the heating due to the propagation of Kelvin and Rossby waves. The magnitude of the response is related to the forcing area. For example, West Pacific anvil CRF (Fig. 6.1b) results in a stronger response than African (Fig. 6.1a) and South American (Fig. 6.1c) anvil CRF. It is possible to speculate from Figs. 6.1a and c that the dynamical response from forcing over Africa and South America counteracts the circulation response from the West Pacific over the Indian Ocean, while the forcing of the three regions in Figs. 6.1a-c has a similar effect over the central Pacific, indicating potential far-field effects of localized anvil heating. The composite effect of anvil CRF over the whole tropics assuming 100% anvil areal coverage (Fig. 6.1d) looks vaguely like the Walker Circulation at upper levels, but is an awkward representation of the large-scale tropical circulation since it does not take into account realistic anvil areal coverage and other components of the total diabatic heating.

In a tropical convective system, latent heating associated with precipitation is the largest term of the total diabatic heating, especially in the system's earlier stages. As the convective system matures, large cloud decks are created and radiative heating becomes more and more significant (Houze 1982). Sensible heating is typically assumed to be small compared to the latent and radiative heating at all stages. Hartmann et al. (1984) were the first to test the sensitivity of the tropical circulation to the vertical profile of total

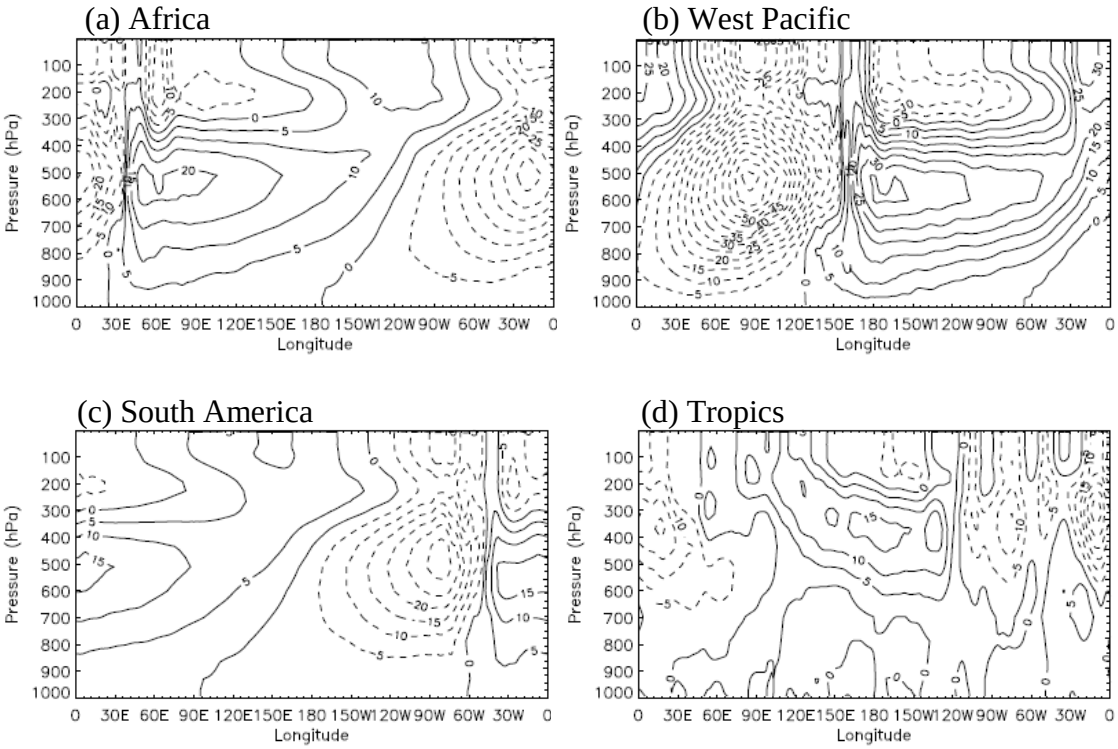

Figure 6. 1 Longitude-height cross sections of zonal mass flux along 20° strip centered on the equator forced by anvil radiative heating assuming 100% areal coverage over (a) Africa, (b) the West Pacific, (c) South America, and (d) the entire tropics. The contour interval is 5×10^{9} kg s^{-1}.

diabatic heating. They forced an idealized climate model with a conventional (convective-only) heating profile and an elevated heating profile that took into account stratiform rain and upper level cloud heating impacts (Fig. 6.2a). The resulting zonal mass flux equatorial cross sections are shown in Fig. 6.2b. Hartmann et al. (1984) argued that the higher circulation center and westward tilt in zonal mass flux over the Pacific Ocean resulting from the elevated heating profile better matched observed zonal mass fluxes. Ensuing studies also argued that tropical cloud CRF has a significant impact on the Walker and Hadley Circulations (Slingo and Slingo 1991, Randall et al. 1989, Sherwood et al. 1994, Bergman and Hendon 2000).

To address this argument in the context of tropical anvil, the anvil radiative heating profile assuming 100% anvil areal coverage was added to the TRMM PR latent heating profile and then used to force the idealized CAM3. Schumacher et al. (2004) estimated the tropics-wide latent heating based on three years (1998-2000) of TRMM PR convective and stratiform rainfall. The same methodology is used here, but the time series is expanded to ten years (1998-2007). Figure 6.3a shows that the tropical mean latent heating heats the depth of the troposphere with a maximum of 1.6 K d^{-1} near 450 hPa with a shape similar to Hartmann et al.'s (1984) conventional profile. The anvil radiative heating profile from Fig. 5.4 (interpolated to the model vertical resolution) increases the latent heating by a factor of three above 600 hPa, with a shape somewhat analogous to Hartmann et al.'s (1984) mature cloud cluster profile.

The resulting model responses (Fig. 6.3b) show a higher circulation center and an increase in a west tilt of the zonal mass flux near 180°E, similar to Hartmann et al. (1984), when the anvil radiative heating is included. However, the increase in height of

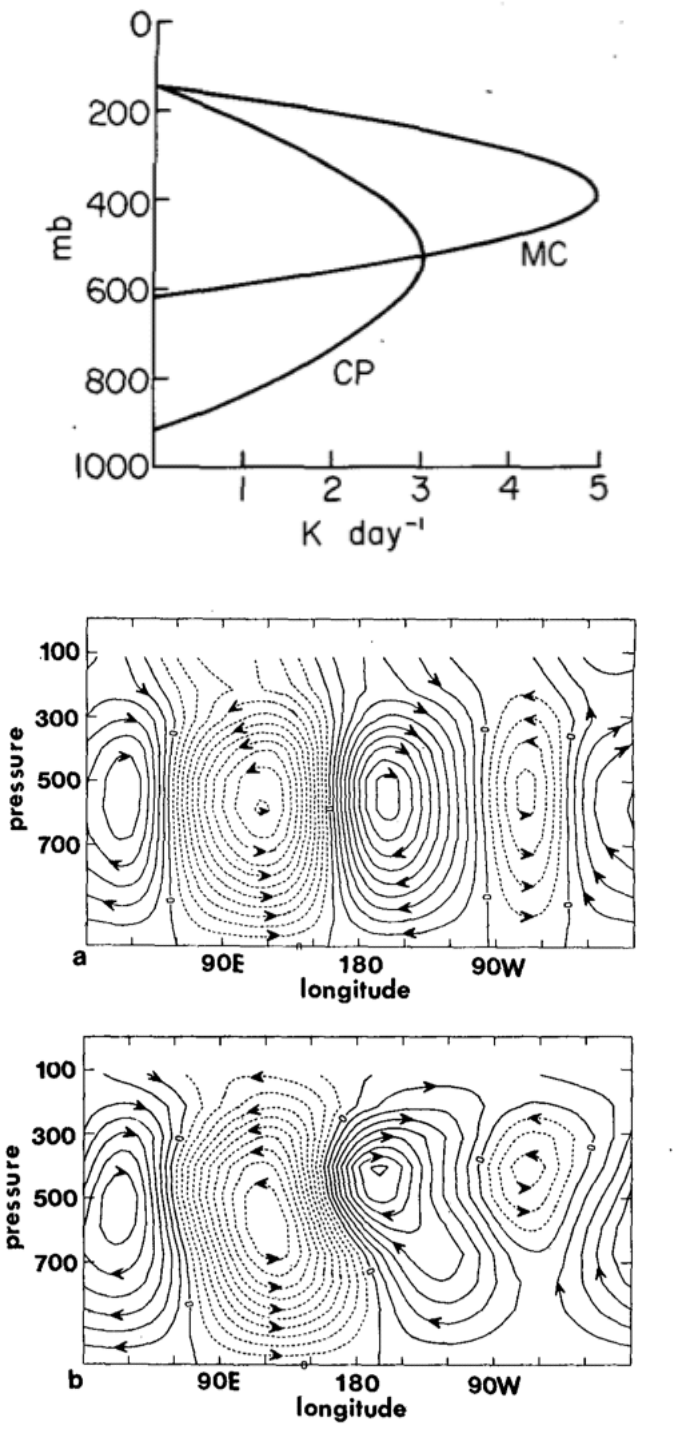

Figure 6. 2 (a) Idealized heating profiles for a conventional deep convective system (CP) and a mature cloud cluster (MC) and (b) model zonal mass flux along the equator forced by the profiles in (a). The contour interval is 5×10^{9} kg s^{-1}. Adapted from Hartmann et al. (1984).

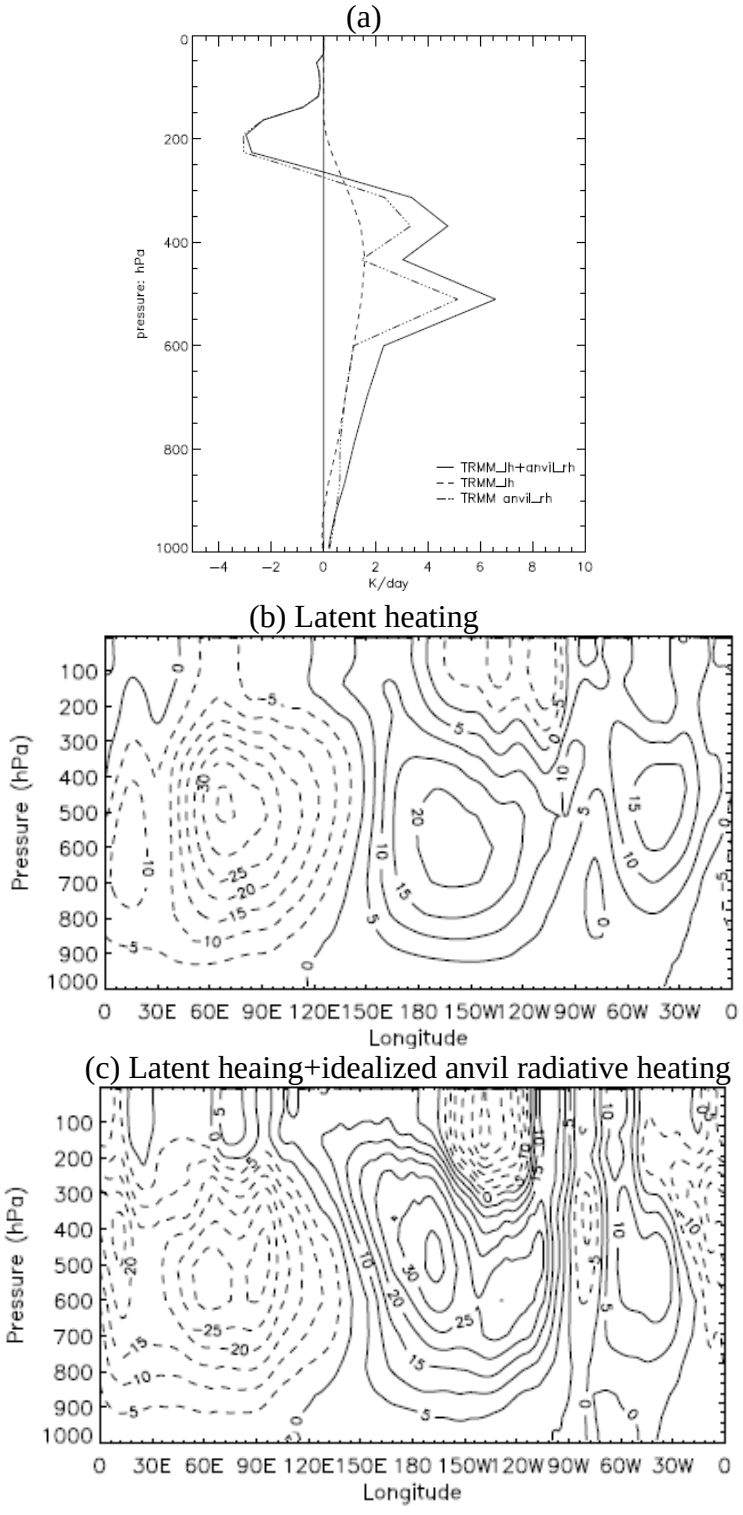

Figure 6. 3 (a) TRMM PR heating profiles assuming 100% areal coverage for the anvil profile and (b) model zonal mass flux along 20° strip centered on the equator forced by the latent heating, and (c) latent heating+anvil radiative heating profiles from (a). The contour interval is 5×10^{9} kg s^{-1}.

the circulation center and the west tilt in zonal mass flux is more extreme than in the NCEP reanalysis cross section (discussed in the next section and shown in Fig. 6.9d) and many other aspects of the circulation response are degraded. This result motivates a careful consideration of realistic radiative contributions to the total diabatic heating profile, especially at upper levels.

6.3 Dynamic response to realistic radiative heating

a. Heating comparisons

It was shown in chapter III that anvil (when corrected for the missing area due to the PR's low sensitivity) generally covers less than 2% of convectively active land regions and even less over warm ocean regions. Therefore, this section adjusts the anvil CRF to reflect observed anvil areal coverage to investigate the importance of anvil radiative heating to the total diabatic heating associated with tropical convective systems. The area-weighted anvil radiative heating is calculated by multiplying the anvil radiative heating profiles that assume 100% anvil cover (Fig. 5.4) by the unconditional anvil areal coverage (Fig. 3.3) times 5 to reflect the portion of the anvil missed by the PR. After taking into account the anvil unconditional areal coverage, the resulting anvil radiative heating (Fig. 6.4, black dashed line) accounts for less than 1% of the latent heating. This result was disappointing since a larger anvil radiative heating impact was expected. Even if the anvil radiative heating calculations were off by a factor of two or three, the large-scale circulation response would be minimal.

To assess potential contributions to the radiative heating by other components of the deep convective cloud system, this study investigated the tropics-wide radiative heating associated with stratiform rain regions and cirrus. The radiative heating profile of

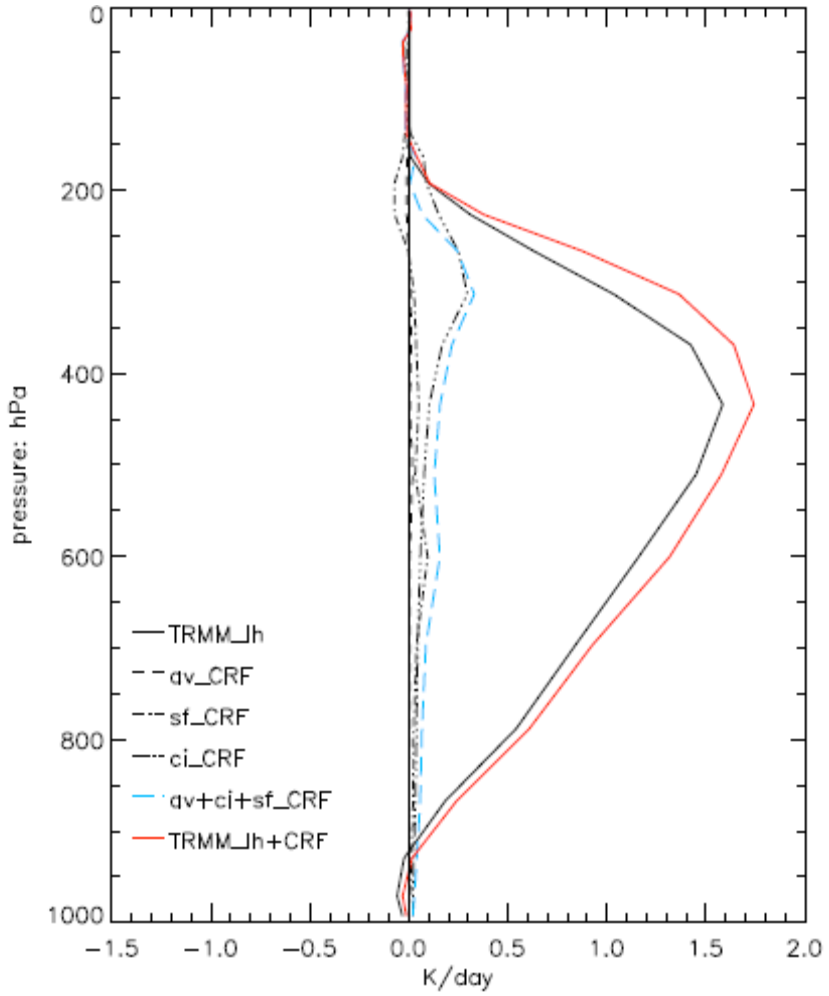

Figure 6. 4 TRMM PR latent and radiative heating profiles from 20°S–20°N during 1998-2007. The latter is weighted by the unconditional area.

stratiform rain is obtained by choosing a profile from the MMCR database that assumes the same vertical extent of mixed anvil but a larger CWC (≥1.5 g m^{-3}). This profile was then multiplied by the unconditional areal coverage of stratiform rain observed by the TRMM PR to obtain the stratiform rain radiative heating across the tropics.

The PR can not observe cirrus, but cirrus observed by CloudSat covers ~15% of the tropics (E. Riley 2009, personal communication). For this study, tropics-wide cirrus heating is roughly estimated by multiplying the mean MMCR cirrus heating profile from Manus (Fig. 5.8) by the anvil unconditional areal coverage (Fig. 3.3a) magnified 250 times to obtain realistic areal coverage of cirrus. This cirrus heating profile is a very rough approximation with the purpose to provide a first order estimate of the radiative contribution to the total diabatic heating. The geographical variability of cirrus needs to be further investigated by observations from radars/lidars with higher sensitivity.

Figure 6.4 shows that the stratiform rain radiative heating (black, dash-dot) is also too small to significantly modify the latent heating. However, cirrus (black, dash-multiple dots) has a maximum heating of 0.3 K d^{-1} at 300 hPa, which contributes significantly to the total heating at upper levels. Thus, when taking account into occurrence, thick anvil and stratiform rain regions contribute marginally to the cloud radiative forcing while cirrus is the largest contributor. The total radiative heating by all three components enhances the latent heating by about 12%.

While the area-weighted radiative heating of thick anvil (the focus of this dissertation) is very small, anvil still retains large local radiative heating values and the CRF of upper tropospheric cloud has been shown to destabilize the cloud layer (Gray and

Jacobson 1977, Webster and Stephens 1980). Anvil also remains an important component in the water budget of tropical convective systems.

To show the geographical modification of the latent heating field by the total radiative heating and to illustrate the forcing distributions used in the next model simulations, Figs. 6.5 and 6.6 show the PR-derived latent heating and radiative heating at 450 and 200 hPa for the entire tropics. As in Schumacher et al. (2004), the heating fields are tapered past 20ºN and 20ºS to avoid sharp discontinuities in the subtropics in the model results. The latent heating at 450 hPa (Fig. 6.5a) is strongest over the Maritime Continent, the West Pacific warm pool, and Central and South America. Radiative heating at the same level (Fig. 6.5b) shows the strongest heating over Africa and Panama. Latent heating at 200 hPa (Fig. 6.6a) is more distributed across the tropical oceans because of the higher stratiform rain fractions (Schumacher and Houze 2003). Weak radiative heating occurs at 200 hPa with larger heating rates over Africa and Panama (Fig. 6.6b). The longitude-height cross sections of latent heating (Fig. 6.7a) and radiative heating (Fig. 6.7b) averaged from 10°S to 10°N show that radiative heating significantly enhances the gradient of latent heating at upper levels over Africa (0-30°E), the Maritime Continent (90-150°E), and South America (70°W).

b. Dynamical response

Schumacher et al. (2004) showed that an elevated latent heating maximum resulting from an increase in stratiform rain fraction strengthened the upper level tropical circulation and that a geographically varying latent heating profile better indicated the tilted zonal circulation characteristics. However, Schumacher et al. also showed that if very high stratiform rain fractions were assumed, the resulting highly elevated latent

(a) Latent heating

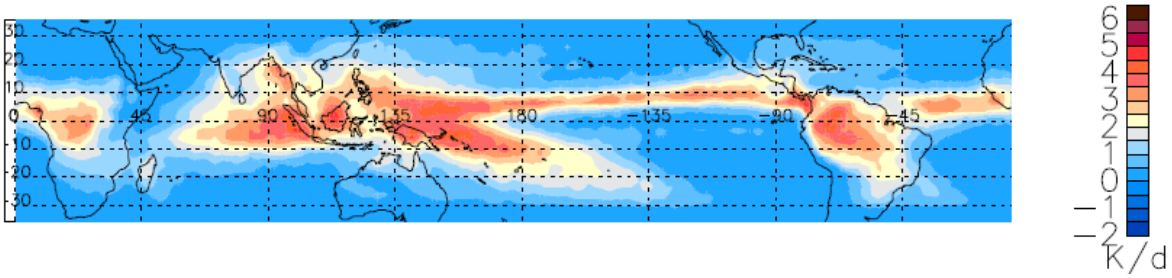

(b) Radiative heating

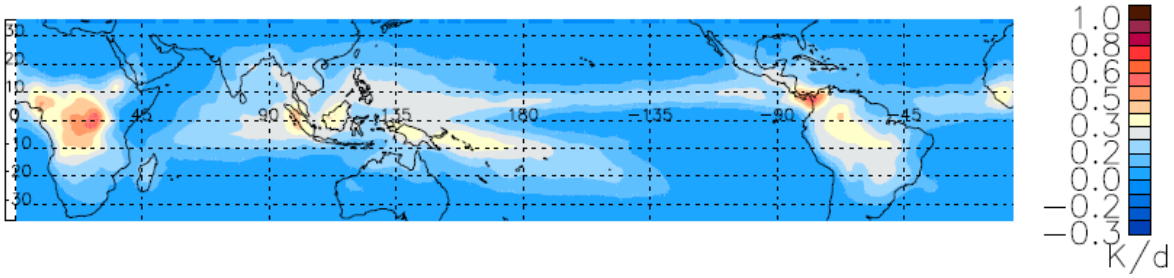

Figure 6. 5 TRMM PR (a) latent heating and (b) area-weighted radiative heating at 450 hPa. Heating outside 20°S and 20°N has been tapered to highlight the tropical heating.

(a) Latent heating

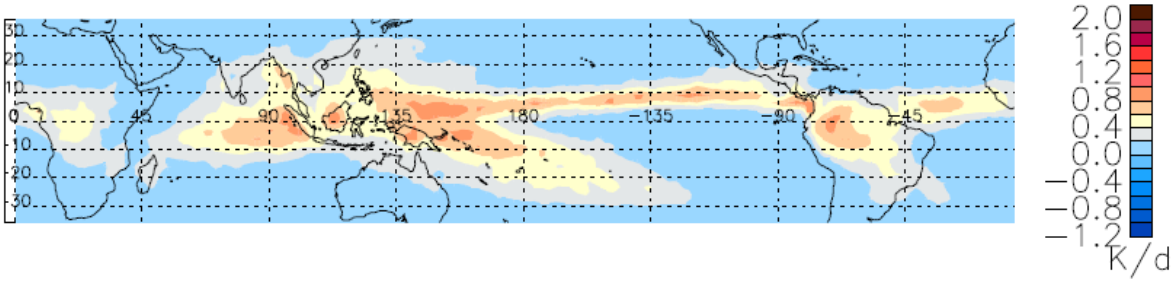

(b) Radiative heating

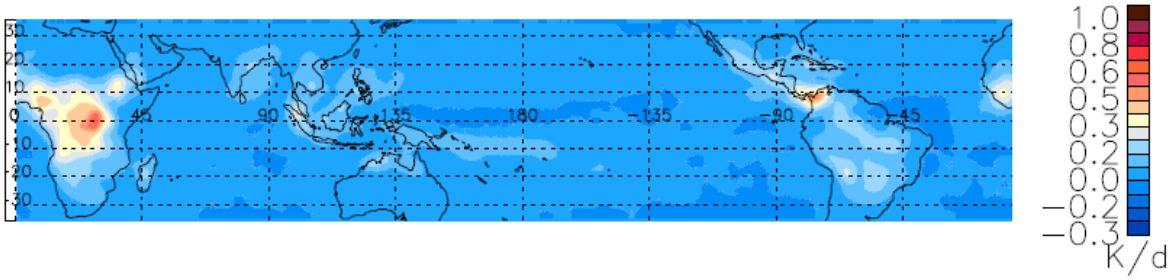

Figure 6. 6 Same as Fig. 6.5 except for 200 hPa.

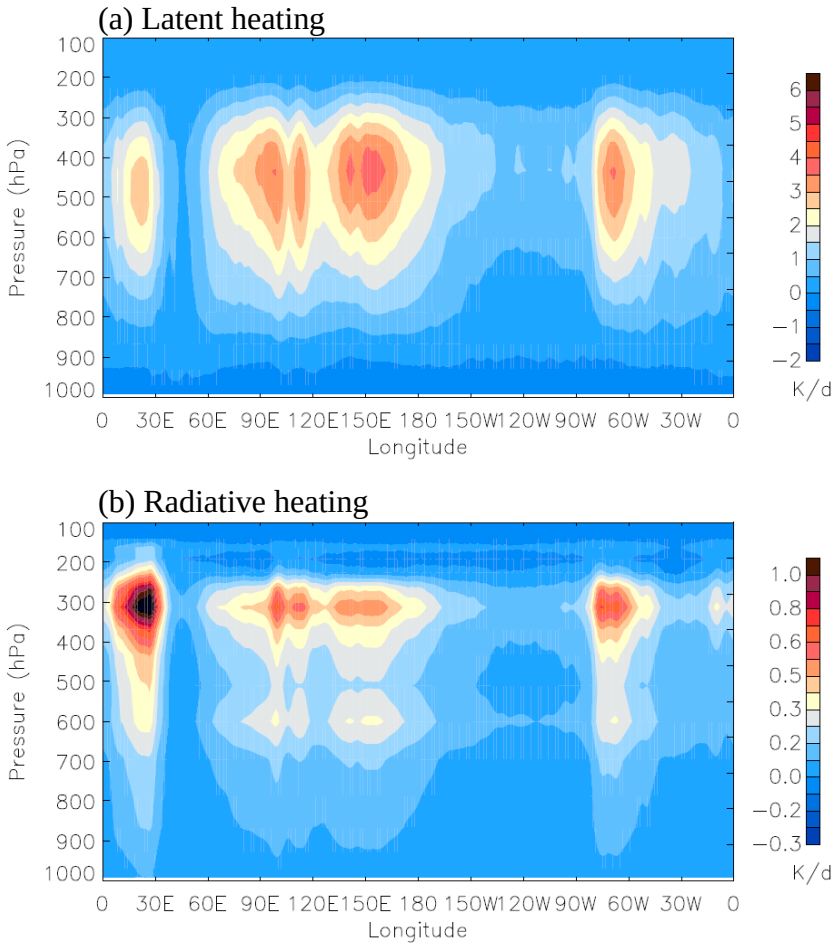

Figure 6. 7 Vertical cross section averaged between 10S°S to 10°N of 10-year mean TRMM PR (a) latent heating (b) area-weighted anvil radiative heating.

heating profile caused an extreme circulation response. Thus, it is important to understand and quantify the factors that affect the upper level heating associated with tropical convective cloud systems in order to determine the convective system impacts on the large-scale circulation. Since streamfunction is related to vorticity ($\zeta = -\nabla^2 \psi$), which is the direct response of heating, and it is smoother than the wind field, streamfunction is usually used to represent the large-scale response of the forcing (Ting and Yu 1998, Schumacher et al. 2004, Hurrell et al. 2006). This study uses the zonal streamfunction anomaly to represent the horizontal large-scale dynamical response to diabatic heating.

Figure 6.8a shows the simulated streamfunction anomalies at 300 hPa forced by the TRMM PR latent heating and indicates broad quadrapole patterns centered on areas of maximum heating (such as the Maritime Continent) seen in previous work (Hartmann et al. 1984, Nigam 1994, Ting and Yu 1998, Schumacher et al. 2004). Similar quadrapole patterns result when the model is forced with the radiative heating alone (Fig. 6.8b), but overall magnitudes are smaller and a more distinct quadrapole center is evident over Africa. Figure 6.8c shows the difference between the model response to latent heating+radiative heating and to latent heating only. Note that Figs.6.8b and c are different because the model response is nonlinearly sensitive to the heating magnitude. The difference in streamfunction anomalies indicates that when adding radiative heating to the latent heating, the circulation response across most of the tropics is slightly enhanced (except for the West and Central Pacific), while more significant enhancement occurs over the East Pacific. Since the heating estimates in this study are observationally

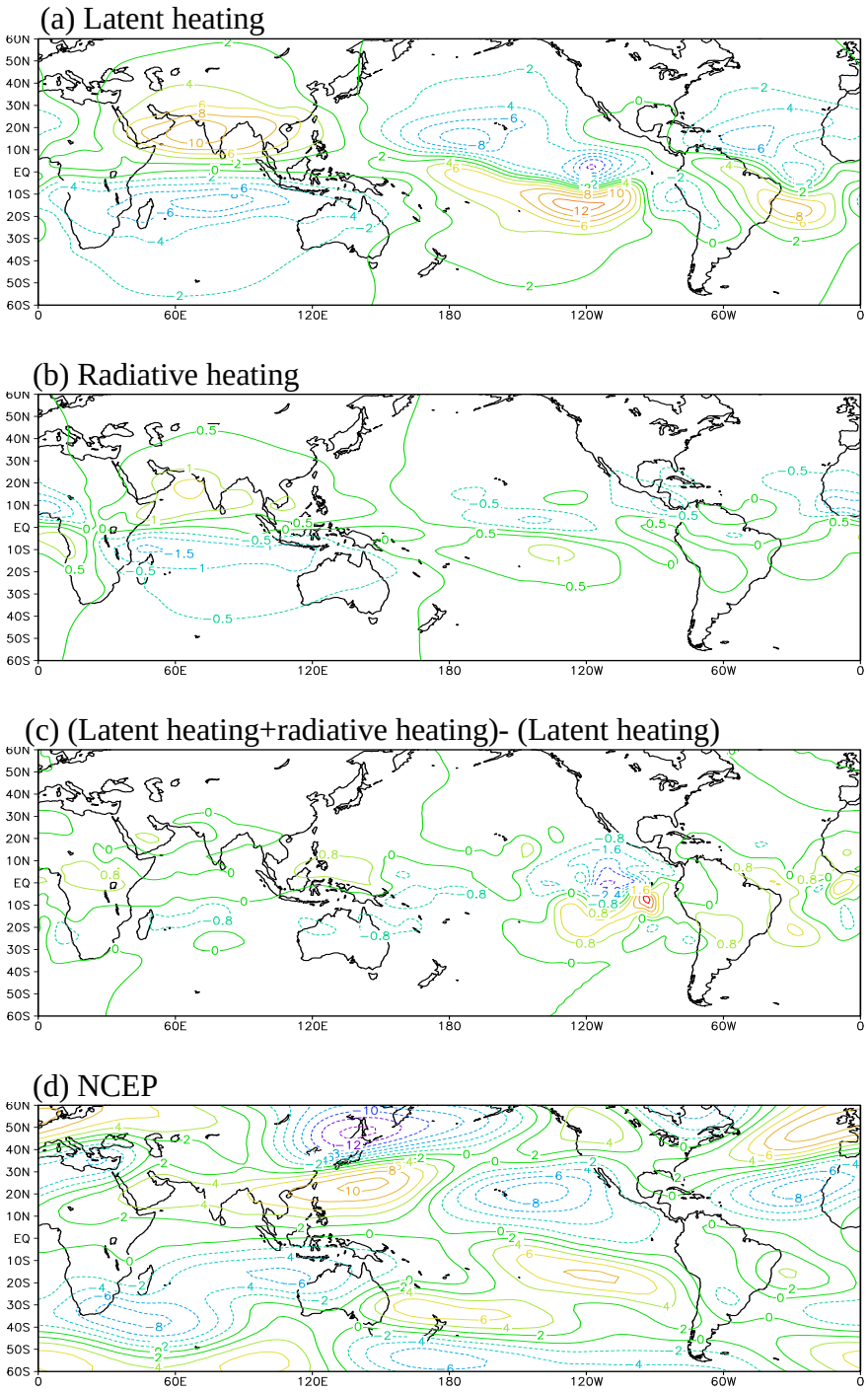

Figure 6. 8 Model streamfunction anomalies at 300 hPa forced by TRMM PR (a) latent heating (b) radiative heating and (c) the difference between the latent heating+radiative heating and latent heating only runs. (d). NCEP reanalysis during 1998-2007. Contour intervals are 2 m^2s^{-1} for (a), (b), (d) and 0.1 m^2s^{-1} for (c).
Streamfunction anomalies for latent heating +radiative heating run is very similar to latent heating only run therefore it is not shown.

based, it is useful to compare the dynamical response with reanalysis data to evaluate the reliability of the estimated heating. Figure 6.8d shows the streamfunction anomaly from 10 years (1998-2007) of monthly NCEP reanalysis data. The response to the latent heating (Fig. 6.8a) shows reasonable agreement with the NCEP reanalysis within the tropics (30°S-30°N).

Figure 6.9a shows the mean zonal mass flux from the TRMM PR latent heating forcing (same as in Fig. 6.3b) and Figs. 6.9b and c show the response to the radiative heating only and to the difference between the latent heating+radiative heating and latent heating only runs, respectively. Figure 6.9d displays the mean zonal mass flux from NCEP reanalysis data. The response to the latent heating (Fig. 6.9a) shows even better agreement with the NCEP tropical zonal circulation, which is consistent with Schumacher et al. (2004). As in the streamfunction anomalies, the radiative heating only response (Fig. 6.9b) shows a similar pattern to the latent heating response, but weaker and with elevated circulation centers. However, this pattern does not bring the latent heating response closer to NCEP. With the addition of the radiative heating to the latent heating (Fig. 6.9c), modification of the zonal mass flux is also observed at upper levels, but the pattern brings the latent heating response more in line with NCEP. In addition, nonlinear features are evident, especially over the East Pacific. As in Fig. 6.8, the response from the radiative heating only run is somewhat exaggerated and nonlinear effects are less pronounced than in the latent heating+radiative heating minus the latent heating only response. Therefore, when assessing the radiative impact of tropical convective systems on the large-scale circulation, the relationship of the radiative heating to the latent heating needs to be taken into account.

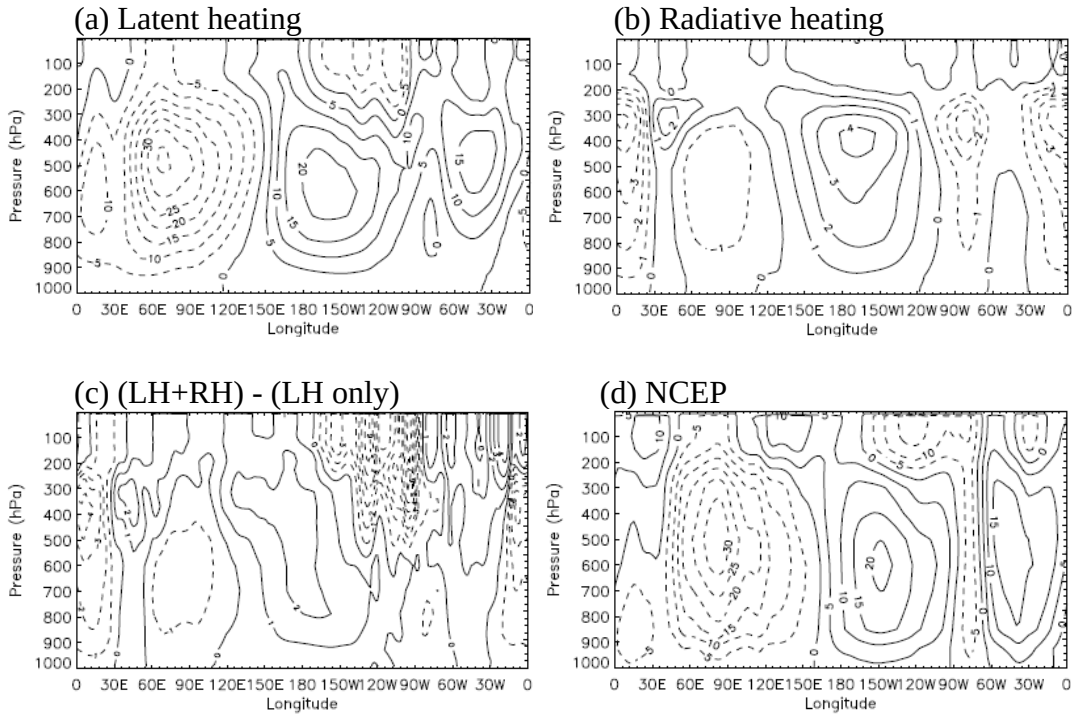

Figure 6. 9 Vertical cross sections of simulated zonal mass flux along 20° strip (in kg s^{-1}) centered on the equator (a) forced by TRMM PR latent heating, (b) forced by TRMM PR radiative heating, and (c) for the difference between the latent heating+radiative heating and latent heating only runs. (d) Ten-year mean (1998–2007) zonal mass flux from monthly NCEP reanalysis zonal winds. The latent heating+radiative heating run is not shown because of its strong similarity to the latent heating only run.

CHAPTER VII

SUMMARY AND DISCUSSION

Studies on the climatological properties of tropical anvil (i.e., thick, non-precipitating cloud associated with deep convection) have been limited due to lack of long-term observations, although anvil is an important component of tropical convective cloud systems. This doctoral work aims to fill this gap by describing the climatology of anvil and anvil properties across the tropics using 10 years of observations from the TRMM PR. In addition, very little is known about the vertical variation of anvil radiative heating and how it impacts the large-scale tropical circulation, which has been shown to be sensitive to vertical and horizontal variations in latent heating associated with precipitation. This doctoral work aims to fill this gap by estimating the tropics-wide anvil radiative heating from the TRMM PR using a look-up table based on DOE ARM MMCR radiative heating retrievals and then forcing an idealized climate model with the resulting heating profiles to determine the sensitivity of the large-scale circulation to tropical anvil.

Across the tropics, PR-observed anvil occurs ~5% of the time and has a conditional areal coverage of 1.5% (this and the following values do not take into account the echo top and area corrections related to the TRMM PR's inability to sense small ice). Average anvil 20-dBZ echo tops range from 8 to 9.5 km with a tropics-wide average of 8.5 km. Average anvil thicknesses range from 1.3 to 3.5 km with a tropics-wide average of 2.7 km. Anvil over land is usually higher and thicker than over ocean. Thick anvil occurs most frequently over Africa, the Maritime Continent, and Panama but has the largest conditional areal coverage over Africa, making Africa a hot spot of anvil

production. When anvil is separated into ice and mixed subtypes (with mixed anvil indicating the possibility of both water and ice hydrometeors being present), further variations in these anvil properties are evident (e.g., mixed anvil is thicker and has lower echo tops than ice anvil and accounts for about two thirds of the total anvil areal coverage).

Anvil properties also experience seasonal and inter-annual variability. Since thick anvil is created by deep convection, this temporal variability is likely due to the variability of the parent deep convection and/or the large-scale environment. For example, anvil echo tops show strong seasonal variability over monsoon regions and anvil occurrence shows strong inter-annual variability over the central Pacific during ENSO events.

Not all convection has the capability to generate thick anvil. Convection that generates anvil is deeper, stronger, and covers more area (as would be found in the mature stage of a tropical convective system), suggesting that each of these factors plays a role in producing and sustaining thick anvil. Anvil to convective rain area ratios range from 1.2/4 to 2.1/4 with more anvil per unit convection over land. In addition, a much wider spread in the frequency distribution of anvil areal coverage versus convective rain area is seen over land compared to ocean. Somewhat surprisingly, stratiform rain area does not seem to be a good predictor of anvil areal coverage.

Stronger wind shear appears to favor enhanced detrainment from the top of the parent convective and stratiform rain regions. The stronger the upper level shear after stratiform rain forms, the more likely anvil is to occur. The upper level TEJ partially explains why more anvil is generated over Africa compared to other tropical land and

ocean locations. The mid to upper troposphere has higher relative humidity (by ~6%) in the presence of anvil, but this likely a result rather than a cause of anvil.

Anvil radiative heating profiles are derived from 10 years of TRMM PR observations using MMCR radiative heating calculations from the DOE ARM site at Manus as the basis of the heating profile look-up table. The TRMM PR underestimated the vertical and horizontal extent of anvil by about 5 km and factor of 4 compared to the CloudSat CPR. These factors are taken into account when calculating the anvil radiative heating. Radiative heating profiles of ice anvil and mixed anvil differ because of differences in cloud vertical extent and optical thickness. The tropics-wide total anvil radiative heating profile shows heating maxima near 6 and 8 km with maximum values of 5 and 3 K d^{-1}, respectively. The maximum cooling of -5 K d^{-1} occurs at 12 km. The anvil radiative heating calculations from CloudSat are consistent with the TRMM PR retrieval, but show weaker maxima (by about 1 K d^{-1}) at higher heights (by about 1 km).

The dynamical core of the NCAR CAM3 was utilized to simulate the tropical dynamical response to the anvil radiative heating assuming 100% areal coverage. The anvil hot spots over Africa, the Maritime Continent, and Central/South America showed far-field effects that combined into something that looks vaguely like an upper level Walker Circulation. Adding the extreme anvil radiative heating values to the TRMM PR latent heating resulted in a response similar to Hartmann et al.'s (1984) mature cloud cluster simulations, i.e., elevated circulation centers and westward tilting zonal mass flux over the Pacific. However, this simulation did not compare favorably to NCEP, motivating an investigation into more realistic radiative heating contributions associated with tropical convective cloud systems.

The modification of the latent heating by the area-weighted anvil radiative heating is extremely small (< 1%), so other components of the radiative heating associated with tropical convective systems were estimated, namely the radiative impact of stratiform rain regions and cirrus. The inclusion of these components increases the mean tropical latent heating profile by about 12% between 600 and 300 hPa. The enhanced upper level heating slightly strengthens the latent heating model response across the tropics (except for the West and Central Pacific), but more significantly over the East Pacific. These modest circulation changes suggest that previous studies may have overemphasized the importance of radiative heating in terms of Walker and Hadley Circulation variations, especially since most previous studies were somewhat more idealized than this work. In addition, assessing the radiative impact of tropical convective systems in isolation does not accurately represent the large-scale response to radiative heating because the relationship of the radiative heating to the latent heating of the convective systems is not taken into account. The response from radiative heating only runs may be exaggerated and nonlinear effects underestimated.

This modeling study uses an observationally based estimate of the anvil, stratiform rain region, and cirrus radiative forcing associated with tropical convective systems rather than relying on the physics of the model. While the dynamical results are reasonable, interactions between the cloud radiative forcing and the large-scale circulation cannot be examined in this framework. In a more localized sense, the elevated heating due to anvil cloud forcing may also destabilize the middle-upper atmosphere (Webster and Stephens 1980, Houze 1981, Ackerman et al. 1988), thus favoring the development of deep convection (Machado and Rossow 1993). A more quantitative

feedback between cloud radiative forcing and the local and large-scale circulation will have to be evaluated by a more interactive modeling framework.

REFERENCES

Ackerman, T. P., K.-N. Liou, F. P. J. Valero, and L. Pfister, 1988: Heating rates in tropical anvils. *J. Atmos. Sci.*, **45,** 1606–1623.

Alcala, C. M., and A. E. Dessler, 2002: Observations of deep convection in the tropics using the Tropical Rainfall Measuring Mission (TRMM) precipitation radar. *J. Geophys. Res.,* **107,** 4792, doi:10.1029/2002JD002457.

Awaka, J., T. Iguchi, H. Kumagai, and K. Okamoto, 1997: Rain type classification algorithm for TRMM Precipitation Radar. *Proc. of the IEEE 1997 Intl. Geoscience and Remote Sensing Sym.*, Aug. 3-8, Singapore, 1633-1635.

Baedi, R.J.P., J.J.M. de Wit, H.W. J. Russchenberg, J.S. Erkelens, and J.P.V. Baptista, 2000: Estimating effective radius and liquid water content from radar and lidar based on the CLARE'98 data-set. *Phys. Chem. Earth*, B25, 1057–1062.

Bergman, J. W., and H. H. Hendon, 2000: Cloud radiative forcing of the low-latitude tropospheric circulation: Linear calculations. *J. Atmos. Sci.,* **57,** 2225–2245.

Black, R. A., 1990: Radar reflectivity-ice water content relationships for use above the melting level in hurricanes. Notes and Correspondence, *J. Appl. Meteor.*, **29**, 955-961.

Brown, E. N., and R. R. Braham Jr., 1963: Precipitation particle measurements in cumulus congestus, *J. Atmos. Sci.*, **20**, 23-28.

Burpee, R. W., 1972: The origin and structure of easterly waves in the lower troposphere of North Africa. *J. Atmos. Sci.,* **29,** 77–90.

Casey, S. P. F., A. E. Dessler, and C. Schumacher, 2007: Frequency of tropical precipitating clouds as observed by the TRMM PR and ICESat/GLAS. *J. Geophys. Res.*, **112**, D14215, doi:10.1029/2007JD008468.

Cetrone, J and R. A. Houze Jr., 2009: Anvil clouds of tropical mesoscale convective systems in monsoon regions: Satellite radar climatology. *Quart. J. Roy. Meteor. Soc.*, **135**, 305-317.

Chen, S.Y., R. A. Houze Jr., and B.E. Mapes, 1996: Multiscale variability of deep convection in relation to large-scale circulation in TOGA COARE. *J. Atmos. Sci.,* **53,** 1380–1409.

Clement, A.C, and B. Soden, 2005: The Sensitivity of the Tropical-Mean Radiation Budget. *J. Climate.,* **18,** 3189-3203.

Colman, R., 2003: A comparison of climate feedbacks in general circulation models. *Clim. Dyn.*, **20**, 865–873.

Comstock, J. M., T. P. Ackerman, and G. G. Mace, 2002: Groundbased lidar and radar remote sensing of tropical cirrus clouds at Nauru Island: Cloud statistics and radiative impacts. *J. Geophys. Res.,* **107,** 4714, doi:10.1029/2002JD002203.

Comstock, J. M, and C. Jakob, 2004: Evaluation of tropical cirrus cloud properties derived from ECMWF model output and ground based measurements over Nauru Island, *Geophys. Res. Lett*., **31**, L10106, doi:10.1029/2004GL019539.

Cook, K. H, 1999: Generation of the African easterly jet and its role in determining west African precipitation, *J. Climate.,* **12,** 1165-1184.

Corti, T., B. P. Luo, Q. Fu, H. V¨omel, and T. Peter, 2006: The impact of cirrus clouds on tropical troposphere-to-stratosphere transport. *Atmos. Chem. Phys*., **6**, 2539–2547.

Fortune M., 1980: Properties of African squall lines inferred from time-lapse satellite imagery. *Mon. Weather Rev*., **108**, 153–168.

Fox, N.I. and A.J. Illingworth, 1997: The retrieval of stratocumulus cloud properties by ground-based cloud radar. *J. Appl Meteor.,* **36,** 485-492.

Frederick, K., and C. Schumacher, 2008: Anvil characteristics as seen by C-POL during the Tropical Warm Pool International Cloud Experiment (TWP-ICE). *Mon. Wea. Rev*., **136**, 206-222.

Futyan J, Del Genio A. 2007. Deep convective system evolution over Africa and the tropical Atlantic. *J. Climate.,* **20,** 5041-5060.

Gray, W., and R. W. Jacobson, 1977: Diurnal variation of deep cumulus convection. *Mon. Wea. Rev.,* **105,** 1171–1188.

Gunn, K. L. S. and J. S. Marshall, 1958: The distribution with size of aggregate snowflakes, *J. Atmos. Sci.,* **15**, 452–461.

Hartmann, D. L., H. H. Hendon, and R. A. Houze Jr., 1984: Some implications of the mesoscale circulations in tropical cloud clusters for large-scale dynamics and climate. *J. Atmos. Sci.,* **41,** 113–121.

Heymsfield, A. J., and A. G. Palmer, 1986: Relationships for deriving thunderstorm anvil ice mass for CCOPE storm water budget estimates, *J. Climate Appl. Meteor*., **25**, 691-702.

Heymsfield, A. J., 2003: Properties of tropical and midlatitude ice cloud particle ensembles. Part II: Applications for mesoscale and climate models, *J. Atmos. Sci.*, **60,** 2592–2611.

Houze Jr. R. A. 1981: Structures of atmospheric precipitation systems – A global survey. *Radio Science,*. **16,** 671-689.

——, 1982: Cloud clusters and large-scale vertical motions in the tropics. *J. Meteor. Soc. Japan*, **60,** 396–410.

——, 1993: *Cloud Dynamics.* San Diego, Academic Press, 573 pp.

——, 1997: Stratiform precipitation in regions of convection: A meteorological paradox? *Bull. Amer. Meteor. Soc.,* **78,** 2179–2196.

Hurrell, J.W., J.J. Hack, A. S. Phillips, J. Caron, and J. Yin, 2006: The Dynamical Simulation of the Community Atmosphere Model Version 3 (CAM3), *J. Climate*, **19**, 2162–2183.

Jakob, C., and G. Tselioudis, 2003: Objective identification of cloud regimes in the Tropical Western Pacific. *Geophys. Res. Lett.*,**30,** 2082, doi:10.1029/2003GL018367.

Jensen, M. P. and A. D. Del Genio, 2003: Radiative and microphysical characteristics of deep convective systems in the tropical western Pacific. *J. Appl. Meteor*., **42**, 1234-1254.

Kozu, T., T. Kawanishi, H. Kuroiwa, M. Kojima, K. Oikawa, H. Kumagai, K. Okamoto, M. Okumura, H. Nakatsuka, and K. Nishikawa, 2001: Development of precipitation radar onboard the Tropical Rainfall Measuring Mission (TRMM) satellite. *IEEE Trans. Geosci. Remote Sens.,* **39,** 102–116.

Krueger, S.K., Q. Fu, K.N. Liou, and H.S Chin, 1995: Improvements of an ice-phase microphysics parameterization for use in numerical simulations of tropical convection. *J. Appl. Meteorol*., **34**, 281-287.

Kummerow, C., W. Barnes, T. Kozu, J. Shiue, and J. Simpson, 1998: The Tropical Rainfall Measuring Mission (TRMM) sensor package. *J. Atmos. Oceanic Technol.,* **15,** 809–817.

Liou, K. N., 1992: Radiation and cloud processes in the atmosphere. Oxford Monographs on Geology and Geophysics No.20, Oxford University Press, Inc., New York, 487pp.

——, 2002: An Introduction to Atmospheric Radiation. 2nd ed., San Diego, Academic Press, 583pp.

Lohmann, U., and E. Roeckner, 1995: Influence of cirrus cloud radiative forcing on climate and climate sensitivity in a general circulation model, *J. Geophys. Res.*, **100**(D8), 16,305–16,323.

Machado, L.A.T. and W.B. Rossow, 1993: Structural characteristics and radiative properties of tropical cloud clusters, *Mon. Wea. Rev.,* **121,** 3234–3260.

Mather J. H., S. A. McFarlane, M. A. Miller, and K. L. Johnson, 2007: Cloud properties and associated radiative heating rate in the tropical western Pacific. *J. Geophys. Res.,***112**, D5201, doi: 10.1029/2006JD007555.

Matrosov, S. Y., 1999: Retrievals of vertical profiles of ice cloud microphysics from radar and IR measurements using tuned regressions between reflectivity and cloud parameters. *J. Geophys. Res.,* **104,** 16 741–16 753.

McFarlane, S.A., and K.F. Evans, 2004a: Cloud and shortwave fluxes at Nauru. Part I: Retrieved cloud properties. *J. Atmos. Sci.,* **61,** 733–744.

——, 2004b: Clouds and shortwave fluxes at Nauru. Part II: Shortwave flux closure. *J. Atmos. Sci.,* **61,** 2602–2615.

McFarlane, S. A., C. N. Long, and D. M. Flynn , 2005: Impact of island induced clouds on surface measurements: Analysis of the ARM Nauru Island effect study data, *J. Appl. Meteorol*., **44**, 1045–1065.

McFarlane S.A., J. H. Mather, and T.P. Ackerman, 2007: Analysis of tropical radiative heating profiles: A comparison of models and observations. *J. Geophys. Res.*, D14218, doi:10.1029/2006JD008290.

Naud, C. M., J.-P. Muller, E. E. Clothiaux, B. A. Baum, and W. P. Menzel, 2005: Intercomparison of multiple years of MODIS, MISR and radar cloud-top heights, *Annales Geophysicae*, **23**, 2415–2424.

Nesbitt, S. W., and E. J. Zipser, 2003: The diurnal cycle of rainfall and convective intensity according to three years of TRMM measurements. *J. Climate,* **16,** 1456–1475.

Nigam, S., 1994: On the dynamical basis for the Asian summer monsoon rainfall–El Nin˜o relationship. *J. Climate,* **7,** 1750–1771.

Petersen, W.A., and S.A. Rutledge, 2001: Regional variability in tropical convection: observations from TRMM. *J. Climate,* **14**, 3566–3586.

Ramanathan, V., E. J. Pitcher, R. C. Malone, and M. L. Blackmon, 1983: The response of a spectral general circulation model to refinements in radiative processes. *J. Amos. Sci.,* **40**, 605-630.

Ramaswamy V., and V. Ramanathan, 1989: Solar absorption by cirrus clouds and the maintenance of the tropical upper troposphere thermal structure. *J. Atmos. Sci.*, **46,** 14, 2293–2310.

Randall, D. A., Harshvardhan, D. A. Dazlich, and T. G. Corsetti, 1989: Interactions among radiation, convection, and largescale dynamics in a general circulation model. *J. Atmos. Sci.* **46,** 1943–1970.

Rasmusson, E. M., and J.M. Wallace, 1983: Meteorological aspects of the El Niño/Southern oscillation, *Science*, **222**(4629), 1195 – 1202.

Riley, E. and B. Mapes, 2009: Unexpected peak near -15C in CloudSat climatology, Submitted to *Geophys. Res. Lett*.

Sassen, K., and L. Liao, 1996: Estimation of cloud content by W-band radar. *J. Appl. Meteorol*., **35,** 2705–2706.

——, Z. Wang, V. I. Khvorostyanov, G. L. Stephens, and A. Bennedetti, 2002: Cirrus cloud ice water content radar algorithm evaluation using an explicit cloud microphysical model, *J. Appl. Meteor.*, **41**, 620-628.

Schumacher, C., and R. A. Houze Jr., 2003a: The TRMM Precipitation Radar's view of shallow, isolated rain. *J. Appl. Meteor.*, **42**, 1519-1524.
——,——, 2003b: Stratiform rain in the tropics as seen by the TRMM Precipitation Radar. *J. Climate*, **16**, 1739-1756.

——,——, 2006: Stratiform precipitation production over sub-Saharan Africa and the tropical East Atlantic as observed by TRMM. *Quart. J. Roy. Meteor. Soc.*, **132**, 2235-2255.

——,——, and I. Kraucunas, 2004: The tropical dynamical response to latent heating estimates derived from the TRMM precipitation radar. *J. Atmos. Sci.,* **61,** 1341–1358.

Sherwood, S. C., V. Ramanathan, T. P. Barnett, M. K. Tyree, and E. Roeckner, 1994: Response of an atmospheric general circulation model to radiative forcing of tropical clouds. *J. Geophys. Res.,* **99,** 20 829–20 846.

Slingo, J. M., and A. Slingo, 1991: The response of a general circulation model to cloud longwave radiative forcing: II. Further studies. *Quart. J. Roy. Meteor. Soc.*, **117**, 333–364.

Soden, B., 2000: The sensitivity of the tropical hydrological cycle to ENSO, *J. Climate,* **13,** 538–549.

Stephens, G.L, D. G. Vane, R. J. Boain, G. G. Mace, K. Sassen, Z. Wang, A. J. Illingworth, E. J. O'Connor, W. B. Rossow, S. L. Durden, S. D. Miller, R. T. Austin,

A. Benedetti, C. Mitrescu, and the Cloudsat science team, 2002: The CloudSat mission and the A-TRAIN: A new dimension of space-based observations of clouds and precipitation. *Bull. Amer. Meteor. Soc.,* **83**, 1771-1790.

——, 2005: Cloud feedbacks in the climate system: A critical review. *J. Climate*, **18**, 237–273.

Thorncroft, C. D., and B. J. Hoskins, 1994a: An idealized study of African easterly waves. I: A linear view. *Quart. J. Roy. Meteor. Soc.,* **120,** 953–982.

Ting, M. F. and L. H. Yu, 1998: Steady response to tropical heating in wavy linear and nonlinear baroclinic models. *J. Amos. Sci*, **55**(24): 3565-3582.

Trenberth, K. E., 1997: The definition of El Niño, *Bull. Amer. Met. Soc*, **78**, 2771-2777.

Wang, H. and R. Fu, 2002: Cross-equatorial flow and seasonal cycle of precipitation over South America, *J. Climate,* **15,** 1591–1608.

Webster, P. J., and G. L. Stephens, 1980: Tropical uppertropospheric extended clouds: Inferences from Winter MONEX. *J. Atmos. Sci.,* **37,** 1521–1541.

Webster, P. J., 1983: Large-scale structure of the tropical atmosphere. *Large Scale Dynamical Processes in the Atmosphere*, B.J Hoskins and R.P Pearce, Eds., London, Academic Press, 397pp.

Wu, R., and J. A. Weinman (1984), Microwave radiances from precipitating clouds containing aspherical ice, combined phase, and liquid hydrometeors, *J. Geophys. Res.,* **89,** 7170–7178.

Yao M. S., and A. D. Del Genio, 1999: Effects of cloud parameterization on the simulation of climate changes in the GISS GCM., *J. Climate*, **12,** 761–779.

Yeh, H. M., N. Prasad, R. A. Mack, and R. F. Adler, 1990: Aircraft microwave observations and simulations of deep convection from 18 to 183 GHz. part II: model results, *J. Atmos. Ocean. Tech*., **7**, 392-410.

Zender. C. S. and J. T. Kiehl, 1997: Sensitivity of climate simulations to radiative effects of tropical anvil structure. *J. Geophys Res.,* **102,** 20. 23793 –23803.

VITA

Name: Wei Li
Address: RM 1204 Eller O&M BLDG, TAMU 3150, College Station, TX, 77843-3150
Email: weili@ariel.met.tamu.edu

Education

Ph.D.	Atmospheric Sciences, Texas A&M University, 2009
M.S.	Climate Dynamics, Chinese Academy of Meteorological Sciences, 2000
B.S.	Meteorology, Nanjing Institute of Meteorology, 1993

Professional Experience

2006-2009	Research Assistant, Texas A&M University
08-12/2004	Visiting scholar, University of California, Los Angeles
12/2003	Visiting scholar, University of Munich, Germany
2002-2006	Research assistant, Chinese Academy of Meteorological Sciences
2000-2002	Graduate research assistant, Chinese Academy of Meteorological Sciences
1993-1997	Weather forecaster, Tianjin Meteorological Observatory

Selected Publications

Li, W. and C. Schumacher, 2009: Tropical Thick Anvil Viewed by the TRMM Precipitation Radar. *In preparation for publication.*

Li, W., C. Schumacher and S. McFarlane, 2009: Radiative heating of the tropical thick anvil. *In preparation for publication.*

Liang Ping, Li Wei, Chen Longxun, He Jinhai and Ren Zejun, 2005: Features and sources of the anomalous moisture transport for the severe summer rainfall over the upper reaches of the Yangtze River, *Acta Meteorologica. Sinica*.,Vol.19,No.2,202-215.

Li Wei, Chen Longxun, 2003: Characteristics of the seasonal variation of the surface total heating over Qinghai-Tibetan Plateau and its surrounding area in summer 1998 and its relationship with the convection over the subtropical area of west Pacific. *Advance in Atmospheric Science*, Vol.20, No.3, 343-348.

Chen L.X., Schmidt F. and Li W., 2003: Characteristics of the atmospheric heat sources and Moisture Sinks over the Qinghai-Tibetan Plateau during the Second TIPEX of Summer 1998 and its Impact on Surrounding Monsoon. *Meteorology and Atmospheric Physics*, Vol. 83, No.1-2, 1-18.

Li Wei, Chen Longxun, 2001: Characteristics of seasonal variation of rainfall over the Tibetan Plateau during summer 1998 and its impact on East Asian weather, *Acta Meteorologica Sinica.*, Vol.15, No.3, 293-309.

Chen Longxun，Li Wei and Zhao Ping, 2001：Impact of winter thermal condition of the Tibetan Plateau on the zonal wind anomaly over equatorial Pacific. *Science in China, Series D.*,Vol. 44 (supp.), 400-409.